LA-14044
Approved for public release;
distribution is unlimited.

An Extended Self-Consistent Viscoplastic Polycrystal Formulation: Application to Polycrystals with Voids

Los Alamos
NATIONAL LABORATORY

This report supersedes LA-UR-03-1193.

Edited by Ryan DeMares, Group IM-1
Photocomposition by Jeanne Bowles, Group IM-1

Los Alamos National Laboratory, an affirmative action/equal opportunity employer, is operated by the University of California for the United States Department of Energy under contract W-7405-ENG-36.

LA-14044
Issued: August 2003

An Extended Self-Consistent Viscoplastic Polycrystal Formulation: Application to Polycrystals with Voids

Ricardo A. Lebensohn
Carlos N. Tomé
Paul J. Maudlin

Los Alamos
NATIONAL LABORATORY

CONTENTS

FIGURES

An Extended Self-Consistent Viscoplastic Polycrystal Formulation: Application to Polycrystals with Voids

Ricardo A. Lebensohn,[*] Carlos N. Tomé,[*] and Paul J. Maudlin[†]

ABSTRACT

In this work we consider the presence of ellipsoidal voids inside polycrystals submitted to large strain deformation. For this purpose, the originally incompressible viscoplastic self-consistent (VPSC) formulation of Lebensohn and Tomé (1993) has been extended to compressible polycrystals. In doing this, both the deviatoric and the spherical components of strain rate and stress are accounted for. Such an extended model allows us to account for the presence of voids and for porosity evolution, while preserving the anisotropy and crystallographic capabilities of the VPSC model. The formulation is adjusted to match Gurson model in the limit of rate-independent isotropic media and spherical voids. We present several applications of this extended VPSC model that address the coupling between texture, plastic anisotropy, void shape, triaxiality, and porosity evolution.

This report contains a detailed and comprehensive derivation of the VPSC polycrystal model and of the equations associated with the theory. Such description is meant to serve as a general reference source for the VPSC formulation and is not limited to the particular case of voided polycrystals.

[*] Materials Science and Technology Division
[†] Theoretical Division

NOTATION

The addition of a spherical component to the formulation makes the associated tensor algebra slightly more complicated. As a consequence, we revise here the notations used in previous publications by the same authors, with the intent of making them more consistent and self-explanatory. The following is a list of the symbols used in this manuscript and their meanings.

a) Vectors

$\overline{x}$	vector of Cartesian space
$\overline{\alpha}$	unitary vector of Fourier space
$\overline{k} = k\overline{\alpha}$	vector of Fourier space
θ and φ	spherical coordinates of the Fourier unit vector $\overline{\alpha}$

b) Velocities, Stresses, and Strain Rates

$\dot{u}_i(\overline{x})$, $\dot{u}_{i,j}(\overline{x})$	velocity and velocity gradient fields
$\dot{\varepsilon}_{ij}(\overline{x})$, $\dot{\varepsilon}_{ij}$, $\dot{E}_{ij}$	strain rate field, average strain rate in each grain, and macroscopic strain rate
$\sigma_{ij}(\overline{x})$, σ_{ij}, Σ_{ij}	Cauchy stress (field, average in each grain, and macroscopic)
$\dot{\varepsilon}^d_{ij}(\overline{x})$, $\dot{\varepsilon}^d_{ij}$, $\dot{E}^d_{ij}$	deviatoric strain rate (field, average in each grain, and macroscopic)
$\dot{\varepsilon}^s(\overline{x}) = \mathrm{tr}\,\dot{\varepsilon}_{ij}(\overline{x})$, $\dot{\varepsilon}^s = \mathrm{tr}\,\dot{\varepsilon}_{ij}$, $\dot{E}^s = \mathrm{tr}\,\dot{E}_{ij}$	dilatation rate (field, average in each grain, and macroscopic)
$\sigma^d_{ij}(\overline{x})$, σ^d_{ij}, Σ^d_{ij}	deviatoric stress (field, average in each grain, and macroscopic)
$\sigma^s(\overline{x}) = \frac{1}{3}\mathrm{tr}\,\sigma_{ij}(\overline{x})$, $\sigma^s = \frac{1}{3}\mathrm{tr}\,\sigma_{ij}$	mean stress (local and average in each grain)
$\Sigma^s = \frac{1}{3}\mathrm{tr}\,\Sigma_{ij}$	mean stress (macroscopic)

$\tilde{\dot{u}}_i(\bar{x})$ local deviation of the velocity field from macroscopic velocity field

$\tilde{\dot{\varepsilon}}^d_{ij}(\bar{x}) = \dot{\varepsilon}^d_{ij}(\bar{x}) - \dot{E}^d_{ij}$, $\tilde{\dot{\varepsilon}}^d_{ij} = \dot{\varepsilon}^d_{ij} - \dot{E}^d_{ij}$

local deviation of deviatoric strain rate (field and average in each grain)

$\tilde{\dot{\varepsilon}}^s(\bar{x}) = \dot{\varepsilon}^s(\bar{x}) - \dot{E}^s$, $\tilde{\dot{\varepsilon}}^s = \dot{\varepsilon}^s - \dot{E}^s$

local deviation of dilatation rate (field and average in each grain)

$\tilde{\sigma}^d_{ij}(\bar{x}) = \sigma^d_{ij}(\bar{x}) - \Sigma^d_{ij}$, $\tilde{\sigma}^d_{ij} = \sigma^d_{ij} - \Sigma^d_{ij}$

local deviation of deviatoric stress (field and average in each grain)

$\tilde{\sigma}^s(\bar{x}) = \sigma^s(\bar{x}) - \Sigma^s$, $\tilde{\dot{\varepsilon}}^s = \sigma^s - \Sigma^s$

local deviation of mean stress (field and average in each grain)

$\dot{E}^d = \left(\frac{2}{3}\dot{E}^d_{ij}\,\dot{E}^d_{ij}\right)^{1/2}$ equivalent macroscopic (Von Mises) deviatoric strain rate

$\Sigma^d = \left(\frac{3}{2}\Sigma^d_{ij}\,\Sigma^d_{ij}\right)^{1/2}$ equivalent macroscopic (Von Mises) deviatoric stress

c) Plasticity-Related Quantities

$m^s_{ij}(\bar{x})$ Schmid tensor of slip system (s) at point $(\bar{x})$

$\tau^s(\bar{x})$ threshold stress of slip system (s) at point $(\bar{x})$

$\dot{\gamma}_o$ strain-rate normalization factor

n rate-sensitivity exponent (inverse of crystal's rate sensitivity)

M_{ijkl} , $\overline{M}_{ijkl}$ viscoplastic compliance (in each grain and macroscopic)

$\dot{\varepsilon}^{do}_{ij}$, $\dot{E}^{do}_{ij}$ back-extrapolated term (in each grain and macroscopic)

L_{ijkl} , $\overline{L}_{ijkl}$ viscoplastic stiffness (in each grain and macroscopic)

K , $\overline{K}$ viscoplastic bulk modulus (in each grain and macroscopic)

d) Green and Eshelby Tensors and Scalars

$\dot{\varepsilon}_{ij}^{d*}(\overline{x})$, $\dot{\varepsilon}_{ij}^{d*}$ deviatoric eigenstrain rate (field and average in each grain)

$\dot{\varepsilon}^{s*}(\overline{x})$, $\dot{\varepsilon}^{s*}$ eigendilatation rate (field and average in each grain)

$\sigma_{ij}^{d*}(\overline{x})$ deviatoric eigenstress field

$f_i^d(\overline{x})$, $f^s(\overline{x})$ deviatoric and spherical inhomogeneity fields

$G_{km}(\overline{x})$, $H_m(\overline{x})$; $\hat{G}_{km}(\overline{k})$, $\hat{H}_m(\overline{k})$

Green functions of velocity and mean stress fields in Cartesian and Fourier spaces, respectively

$\tilde{\dot{u}}_{i,j}^d(\overline{x})$, $\tilde{\dot{u}}_{i,j}^d$ contribution of deviatoric components to local deviation of velocity gradient (field and average in the grain)

$\tilde{\dot{u}}_{i,j}^s(\overline{x})$, $\tilde{\dot{u}}_{i,j}^s$ contribution of spherical components to local deviation of velocity gradient (field and average in the grain)

T_{ijkl}^d , T_{ij}^s deviatoric and spherical Green interaction tensors

S_{ijkl}^d , S_{ij}^s deviatoric and spherical Eshelby tensors

$\Psi = \mathrm{tr}(S_{ij}^s)$ Eshelby factor (trace of spherical Eshelby tensor)

Ψ_v , Ψ_g Eshelby factor of voids and grains, respectively

$\beta_{ij} = \frac{S_{ij}^s}{\Psi} - \frac{\delta_{ij}}{3}$ Eshelby coupling tensor

e) Interaction and Localization Tensors and Factors

$\tilde{M}_{ijkl}$, $\tilde{\beta}_{kl}$ deviatoric and coupling interaction tensors

B_{ijkl} , Φ_{ij} , B^s stress localization tensors

A_{ijkl} , Ω_{ij} , A^s strain-rate localization tensors

$\tilde{K}$ spherical interaction factor

$\tilde{K}_v$, $\tilde{K}_g$	spherical interaction factor of voids and grains, respectively
$\Sigma_{ij}^{d\bullet}$, $\Sigma^{s\bullet}$, $\dot{E}_{ij}^{d\bullet}$, $\dot{E}^{s\bullet}$	reference stress and strain-rate magnitudes needed to derive generalized self-consistent relations

f) Miscellaneous

Φ	porosity (void volume fraction)
a, b, c	principal radii of the ellipsoid
Y	equivalent (Von Mises) yield stress of solid phase
$X = \frac{\Sigma^s}{\Sigma^d}$	stress triaxiality

1. INTRODUCTION

The evolution of porosity is of relevance for assessing damage during both quasi-static and high strain-rate deformation of metallic aggregates. The Gurson (1977) criterion, which provides a constitutive relation between yield stress and strain rate in voided materials, is widely used in simulations of metal deformation under complex boundary conditions (e.g., Johnson and Addessio, 1988). The Gurson constitutive law follows from an upper-bound solution of a unit cell problem, based on the simplifying assumptions of elastically rigid, isotropy, perfectly plastic, rate-independent matrix plastic behavior, spherical voids, and no void interaction. Such assumptions do not adequately represent many situations in which the anisotropy of the material response or the void shape or rate effects may play a role. As a consequence, modifications of the Gurson model have been proposed to address some of these issues, e.g, void shape (Lee and Mear, 1992; Golaganu et al., 1993, 1994), matrix anisotropy (Chen et al., 2000), rate sensitivity (Lee and Mear, 1992; Addessio and Johnson, 1993; Liu et al., 2002; Chen et al., 2002) and void interaction (Tveergard, 1982).

Ponte Castañeda and coworkers (Ponte Castañeda et al., 1994; Kailasam et al., 1997a,b), on the other hand, have developed a model based on the variational formulation of Ponte Castañeda (1991) to predict the behavior of porous rate-sensitive materials with isotropic phases, taking into account the field fluctuations induced by the presence of voids and the anisotropy induced by void-shape evolution. The best performance of this model is obtained at low void concentration and low triaxiality. Such formulation was implemented inside an elastoplastic FEM code to account for the evolution of porosity and the development of anisotropy due to changes in the shape and orientation of the voids during deformation (Kailasam et al., 2000). Later, Ponte Castañeda (1996) developed a second variational formulation that yields estimates that are exact to second order in the fluctuation of properties between phases, and therefore are specially suitable for porous materials. However, this second-order procedure does not take into account the field fluctuations and therefore is not accurate for cases near percolation or of high triaxiality. More recently, Ponte Castañeda (2002a,b) developed a new formulation that combines the main advantages of the former models (i.e., takes into account the field fluctuations and is exact to second order in the contrast), which can be applied to the high triaxiality, void-concentration case.

The study of the interplay between texture and anisotropy of polycrystalline materials motivated the development of numerous polycrystal models. Such models allow us to predict the evolution of anisotropy, texture, and hardening during plastic deformation of an aggregate of anisotropic grains. When the single crystal anisotropy is severe, self-consistent formulations should be used instead of the simpler upper-bound formulation (Taylor, 1938) to obtain accurate results. In particular, the fully anisotropic viscoplastic self-consistent (VPSC) model developed by Lebensohn and Tomé (1993), based on the original Molinari et al. (1987) isotropic formulation, has been successfully used in the last ten years to describe the constitutive response of a variety of anisotropic systems under diverse loading conditions. Recently, VPSC has been interfaced with FEM codes to describe the forming of Zr and Zr alloys (Logé et al., 1998; Tomé et al., 2001) under complex boundary conditions.

Although the VPSC polycrystal theories have also been extended to multiphase polycrystals (e.g., Lebensohn and Canova, 1997) until now no model was available to treat the large-strain deformation of voided polycrystals, i.e., an extreme case of a two-phase aggregate with infinite contrast between phases. A formulation with such characteristics would be useful, for example, to predict the behavior of anisotropic materials submitted to dynamic loading conditions with the ultimate goal of building a numerical interface with dynamic FEM codes. With this in mind, we present here a 3-D VPSC model for polycrystals with preexisting voids that allows us to consider the full anisotropy associated with morphologic evolution of voids and grains and with crystallographic texture development in the aggregate, as well as rate effects. The model applies to the stage of void growth but not to the previous stage of void nucleation nor the subsequent stage of void coalescence.

The formulation is a generalization of the incompressible fully anisotropic VPSC model of Lebensohn and Tomé (1993) and Lebensohn et al. (1998). This model treats each grain as a viscoplastic ellipsoidal inclusion embedded in a homogeneous effective medium (HEM). Since both the inclusion and the HEM are anisotropic and incompressible, the model was formulated in the deviatoric 5-dimensional space. In the present extension, cavities are still treated as ellipsoidal inclusions but the assumption of incompressibility does not apply to the voids nor to the HEM (the inclusions representing grains, however, remain incompressible). Dilatation and hydrostatic pressure have to be accounted for, and they represent the sixth dimension of the problem.

An important requirement for this extended VPSC formulation is that it should reproduce Gurson's results for the case of rate-insensitive isotropic aggregates with spherical voids, for different triaxialities and porosities. The procedure used here for adjusting the extended VPSC formulation to the Gurson limit is inspired by the work of Ponte Castañeda (2002a,b), and is based on adjusting the local linearized behavior in the grains to implicitly take into account the field fluctuations in the grains due to the presence of voids. To acomplish this, it has been necessary to generalize the tangent VPSC model of Lebensohn and Tomé (1993) to allow for an ad hoc linearization of the grain's constitutive response, as originally proposed by Masson et al. (2000) in their affine formulation.

In the next section, we describe the formulation and discuss its assumptions in detail. Next, we illustrate some of the capabilities of the model with several applications. First, we make a comparison with the Gurson model, after which we study the role of texture, rate sensitivity, and void morphology (shape) upon porosity evolution and stress-strain response. We consider both fcc and hcp polycrystals in this analysis.

2. EXTENDED VPSC MODEL

2.1. Local Constitutive Behavior and Homogenization

Let us consider an aggregate consisting of grains (material phase) and cavities (void phase). The deviatoric part of the viscoplastic constitutive behavior of the material phase at local level is described by means of the nonlinear rate-sensitivity equation

$$\dot{\varepsilon}_{ij}^{d}(\bar{x}) = \dot{\gamma}_o \sum_s m_{ij}^{s}(\bar{x}) \left(\frac{m_{kl}^{s}(\bar{x})\, \sigma_{kl}^{d}(\bar{x})}{\tau^{s}(\bar{x})} \right)^{n} , \qquad (1)$$

where $\dot{\varepsilon}_{ij}^{d}(\bar{x})$ and $\sigma_{kl}^{d}(\bar{x})$ are the deviatoric strain rate and stress fields, $m_{ij}^{s}(\bar{x})$ and $\tau^{s}(\bar{x})$ are the Schmid tensor and the threshold stress of slip (s), $\dot{\gamma}_o$ is a normalization factor, and n is the rate-sensitivity exponent. Linearizing Eq. (1) inside the domain of a grain and adding a linear relation between the spherical components of stress and strain rate gives

$$\dot{\varepsilon}_{ij}^{d}(\bar{x}) = M_{ijkl}\, \sigma_{kl}^{d}(\bar{x}) + \dot{\varepsilon}_{ij}^{do} , \qquad (2a)$$

$$\dot{\varepsilon}^{s}(\bar{x}) = K^{-1}\, \sigma^{s}(\bar{x}) , \qquad (2b)$$

where $\dot{\varepsilon}_{ij}^{d}(\bar{x})$, $\dot{\varepsilon}^{s}(\bar{x}) = \text{tr}\,\dot{\varepsilon}_{ij}(\bar{x})$ and $\sigma_{ij}^{d}(\bar{x})$, $\sigma^{s}(\bar{x}) = \frac{1}{3}\text{tr}\,\sigma_{ij}(\bar{x})$ are the deviatoric and spherical components of the local fields, and M_{ijkl}, $\dot{\varepsilon}_{ij}^{do}$ and K are the grain's viscoplastic compliance, back-extrapolated term, and viscoplastic bulk modulus, respectively. Concerning the linearization in the equation that relates the deviatoric components, in the material phase, M_{ijkl} and $\dot{\varepsilon}_{ij}^{do}$ can be chosen differently. While the original VPSC formulation (Molinari et al., 1987; Lebensohn and Tomé, 1993) was restricted to the assumption of a tangent linearization of the local behavior, Masson et al. (2000) generalized these kinds of self-consistent formulations to arbitrary linearized behaviors by means of the so-called affine procedure. In what follows, we will adopt Masson et al.'s affine linearization scheme since it provides the required flexibility to take into account the effect of porosity on the local behavior of the material phase, leaving for later the discussion regarding which is the best choice of the linear moduli in the case of voided polycrystals.

Equation (2b), which relates the spherical components, it expands the scope of the constitutive response, and the derivation that follows is general and has application beyond the specific case of voided polycrystals. For the grains of an incompressible solid phase, it holds that $K \to \infty$, and Eq. (2b) just states the condition of incompressibility. Solving simultaneously Eqs. (2a) and (2b) allowed us (Lebensohn et al., 1998) to solve the problem of the incompressible inclusion without using the penalty method, which consists in assuming a very small (rather than null) compressibility (Hutchinson, 1976). As for the infinitely compliant void phase, we can write expressions formally equivalent to Eq. (2), taking $M_{ijkl} \to \infty$ and $K = 0$.

Performing homogenization on this heterogeneous medium consists in assuming pseudo-linear constitutive relations analogous to (2) at the effective medium (polycrystal) level

$$\dot{E}_{ij}^{d} = \overline{M}_{ijkl}\,\Sigma_{kl}^{d} + \dot{E}_{ij}^{do}\ , \tag{3a}$$

$$\dot{E}^{s} = \overline{K}^{-1}\,\Sigma^{s}\ , \tag{3b}$$

where $\dot{E}_{ij}^{d}$, Σ_{ij}^{d}, $\dot{E}^{s}$, and Σ^{s} are overall (macroscopic) deviatoric and spherical magnitudes and $\overline{M}_{ijkl}$, $\dot{E}_{ij}^{do}$, and $\overline{K}$ are the macroscopic viscoplastic compliance, back-extrapolated term and

viscoplastic bulk modulus, respectively. The latter moduli are unknown *a priori* and should be adjusted self-consistently. Due to the presence of voids, the effective viscoplastic bulk modulus $\overline{K}$ has a finite nonzero value even if the solid material is incompressible. Invoking the concept of the equivalent inclusion (Mura, 1988), the local constitutive behavior can be rewritten in terms of the homogeneous macroscopic moduli so that the inhomogeneity is hidden inside a fictitious transformation rate (referred to as eigenstrain rate in what follows) as

$$\dot{\varepsilon}_{ij}^{d}(\bar{x}) = \overline{M}_{ijkl}\,\sigma_{kl}^{d}(\bar{x}) + \dot{E}_{ij}^{do} + \dot{\varepsilon}_{ij}^{d*}(\bar{x}), \tag{4a}$$

$$\dot{\varepsilon}^{s}(\bar{x}) = \overline{K}^{-1}\sigma^{s}(\bar{x}) + \dot{\varepsilon}^{s*}(\bar{x}), \tag{4b}$$

where $\dot{\varepsilon}_{ij}^{d*}(\bar{x})$ and $\dot{\varepsilon}^{s*}(\bar{x})$ are the deviatoric eigenstrain-rate field and a newly defined eigendilatation-rate field, respectively, which follow from replacing the inhomogeneity by an equivalent inclusion. Rearranging and subtracting (3) from (4) gives

$$\tilde{\sigma}_{ij}^{d}(\bar{x}) = \overline{L}_{ijkl}\left(\tilde{\dot{\varepsilon}}_{kl}^{d}(\bar{x}) - \dot{\varepsilon}_{kl}^{d*}(\bar{x})\right), \tag{5a}$$

$$\tilde{\sigma}^{s}(\bar{x}) = \overline{K}\left(\tilde{\dot{\varepsilon}}^{s}(\bar{x}) - \dot{\varepsilon}^{s*}(\bar{x})\right), \tag{5b}$$

where the ~ quantities are local deviations from macroscopic values and $\overline{L}_{ijkl} = \overline{M}_{ijkl}^{-1}$.

Combining (5) with the equilibrium condition

$$\sigma_{ij,j}(\bar{x}) = \tilde{\sigma}_{ij,j}(\bar{x}) = \tilde{\sigma}_{ij,j}^{d}(\bar{x}) + \tilde{\sigma}_{,i}^{s}(\bar{x}), \tag{6}$$

and using the relation between strain rate and velocity gradient, i.e., $\tilde{\dot{\varepsilon}}_{ij}(\bar{x}) = \frac{1}{2}\left(\tilde{\dot{u}}_{i,j}(\bar{x}) + \tilde{\dot{u}}_{j,i}(\bar{x})\right)$, we obtain

$$\overline{L}_{ijkl}\,\tilde{\dot{u}}_{k,lj}(\bar{x}) + \tilde{\sigma}_{,i}^{s}(\bar{x}) + f_{i}^{d}(\bar{x}) = 0, \tag{7a}$$

$$\overline{K}\,\tilde{\dot{u}}_{k,k}(\bar{x}) - \tilde{\sigma}^{s}(\bar{x}) + f^{s}(\bar{x}) = 0, \tag{7b}$$

where the fictitious forces associated with the heterogeneity are

$$f_{i}^{d}(\bar{x}) = -\overline{L}_{ijkl}\dot{\varepsilon}_{kl,j}^{d*}(\bar{x}) = \sigma_{ij,j}^{d*}(\bar{x}), \tag{8}$$

$$f^{s}(\bar{x}) = -\overline{K}\dot{\varepsilon}^{s*}(\bar{x}). \tag{9}$$

The field $\sigma_{ij}^{d*}(\bar{x}) = -\bar{L}_{ijkl}\dot{\varepsilon}_{kl}^{d*}$ defined in (8) will be called in what follows eigenstress field.

2.2. Green Function Method and Fourier Transform Solution

System (7) consists of four differential equations with four unknowns: three are the components of velocity deviation vector $\tilde{u}_i(\bar{x})$ and one is the mean stress deviation $\tilde{\sigma}^s(\bar{x})$. Formally, system (7) can be expressed as

$$D_{iq}\, g_q(\bar{x}) + f_i(\bar{x}) = 0 \qquad (i,q = 1,4)\ , \tag{10}$$

where the 4-dimensional unknown and inhomogeneity vector fields are, respectively,

$$\bar{g}(\bar{x}) = \left(\tilde{u}_1(\bar{x}), \tilde{u}_2(\bar{x}), \tilde{u}_3(\bar{x}), \tilde{\sigma}^s(\bar{x})\right), \tag{11}$$

$$\bar{f}(\bar{x}) = \left(f_1^d(\bar{x}), f_2^d(\bar{x}), f_3^d(\bar{x}), f^s(\bar{x})\right), \tag{12}$$

and the differential operator D is given by:

$$D = \begin{bmatrix} \bar{L}_{1r1s}\dfrac{d^2}{dx_r dx_s} & \bar{L}_{1r2s}\dfrac{d^2}{dx_r dx_s} & \bar{L}_{1r3s}\dfrac{d^2}{dx_r dx_s} & \dfrac{d}{dx_1} \\ \bar{L}_{2r1s}\dfrac{d^2}{dx_r dx_s} & \bar{L}_{2r2s}\dfrac{d^2}{dx_r dx_s} & \bar{L}_{2r3s}\dfrac{d^2}{dx_r dx_s} & \dfrac{d}{dx_2} \\ \bar{L}_{3r1s}\dfrac{d^2}{dx_r dx_s} & \bar{L}_{3r2s}\dfrac{d^2}{dx_r dx_s} & \bar{L}_{3r3s}\dfrac{d^2}{dx_r dx_s} & \dfrac{d}{dx_3} \\ \bar{K}\dfrac{d}{dx_1} & \bar{K}\dfrac{d}{dx_2} & \bar{K}\dfrac{d}{dx_3} & -1 \end{bmatrix}. \tag{13}$$

A system of N linear differential equations with N unknown functions and an inhomogeneity term such as (10) can be solved using a tensorial extension of the Green function method, which is explained below. Assume that $G_{qm}(\bar{x})$ is the Green tensor, which solves the auxiliary problem of a unitary inhomogeneity field with a single nonvanishing m-component applied at $\bar{x} = 0$,

$$D_{iq}\, G_{qm}(\bar{x}) + \delta(\bar{x})\delta_{im} = 0 \qquad (i,q,m = 1,4)\ , \tag{14}$$

where $\delta(\bar{x})$ is Dirac's delta function and δ_{im} is the Kronecker delta. Then the solution of system (10) is given by the convolution integral

$$g_q(\bar{x}) = \int G_{qm}(\bar{x} - \bar{x}')f_m(\bar{x}')d\bar{x}' \quad . \tag{15}$$

The proof is as follows:

$$\begin{aligned} D_{iq}\, g_q(\bar{x}) &= D_{iq}\int G_{qm}(\bar{x} - \bar{x}')f_m(\bar{x}')d\bar{x}' = \int D_{iq}\, G_{qm}(\bar{x} - \bar{x}')f_m(\bar{x}')d\bar{x}' = \\ &= \int -\delta(\bar{x} - x')\delta_{im} f_m(\bar{x}')d\bar{x}' = -f_i(\bar{x}). \end{aligned} \tag{16}$$

In our particular case, if $G_{km}(\bar{x})$ and $H_m(\bar{x})$ denote the Green functions associated with $\tilde{u}_i(\bar{x})$ and $\tilde{\sigma}^s(\bar{x})$, the auxiliary problem (14) is written as

$$\bar{L}_{ijkl}\, G_{km,lj}(\bar{x}) + H_{m,i}(\bar{x}) + \delta_{im}\,\delta(\bar{x}) = 0\,, \tag{17a}$$

$$\bar{K}\, G_{km,k}(\bar{x}) - H_m(\bar{x}) + \delta_{4m}\,\delta(\bar{x}) = 0\,. \tag{17b}$$

(i,j,k,l = 1,3 ; m = 1,4)

System (17) can be solved using the Fourier transform method. The direct and inverse Fourier transforms of the Green functions G_{km} and H_m are defined by[‡]

$$\hat{G}_{km}(\bar{k}) = \int G_{km}(\bar{x})\exp(i\bar{k}\bar{x})d\bar{x}\,, \tag{18a}$$

$$G_{km}(\bar{x}) = \frac{1}{8\pi^3}\int \hat{G}_{km}(\bar{k})\exp(-i\bar{k}\bar{x})d\bar{k}\,, \tag{18b}$$

$$\hat{H}_m(\bar{k}) = \int H_m(\bar{x})\exp(i\bar{k}\bar{x})d\bar{x}\,, \tag{19a}$$

$$H_m(\bar{x}) = \frac{1}{8\pi^3}\int \hat{H}_m(\bar{k})\exp(-i\bar{k}\bar{x})d\bar{k}\,. \tag{19b}$$

In addition, Dirac's delta function can be expressed as

$$\delta(\bar{x}) = \frac{1}{8\pi^3}\int \exp(-i\bar{k}\bar{x})d\bar{k} \quad . \tag{20}$$

Replacing Eqs. (18)–(20) in (17) and taking derivatives with respect to $\bar{x}$ inside the integrals, transforms the differential system into an algebraic system:

$$-\alpha_j\,\alpha_l\,\bar{L}_{ijkl}\, k^2\hat{G}_{km}(\bar{k}) - \alpha_i\, ik\hat{H}_m(\bar{k}) + \delta_{im} = 0\,, \tag{21a}$$

$$\bar{K}(-i\alpha_k)k\hat{G}_{km}(\bar{k}) - \hat{H}_m(\bar{k}) + \delta_{4m} = 0\,, \tag{21b}$$

[‡] In what follows, the letter "i" is used both to denote the unit imaginary number and as a tensor index.

where k and $\overline{\alpha}$ are the modulus and the unit vector associated with a point of Fourier space $\overline{k}$ (i.e., $\overline{k} = k\overline{\alpha}$), respectively. Multiplying (21a) and (21b) by (–1) and $(ik\overline{K}^{-1})$, respectively, we obtain

$$\alpha_j \alpha_l \overline{L}_{ijkl}\, k^2 \hat{G}_{km}(\overline{k}) + \alpha_i\, ik\hat{H}_m(\overline{k}) = \delta_{im}\ , \tag{22a}$$

$$\alpha_k\, k^2 \hat{G}_{km}(\overline{k}) - \overline{K}^{-1}\, ik\hat{H}_m(\overline{k}) = -\overline{K}^{-1} ik\delta_{4m}\ . \tag{22b}$$

Calling $A^d_{ik} = \alpha_j \alpha_l \overline{L}_{ijkl}$, system (22) can be expressed as a matrix product $A = B \times C$, where A, B, and C are 4×4 matrices given by

$$A = \left[\begin{array}{cccc} A^d_{11} & A^d_{12} & A^d_{13} & \alpha_1 \\ A^d_{21} & A^d_{22} & A^d_{23} & \alpha_2 \\ A^d_{31} & A^d_{32} & A^d_{33} & \alpha_3 \\ \alpha_1 & \alpha_2 & \alpha_3 & -\overline{K}^{-1} \end{array}\right] \left|\begin{array}{cccc} k^2\hat{G}_{11} & k^2\hat{G}_{12} & k^2\hat{G}_{13} & k^2\hat{G}_{14} \\ k^2\hat{G}_{21} & k^2\hat{G}_{22} & k^2\hat{G}_{23} & k^2\hat{G}_{24} \\ k^2\hat{G}_{31} & k^2\hat{G}_{32} & k^2\hat{G}_{33} & k^2\hat{G}_{34} \\ ik\hat{H}_1 & ik\hat{H}_2 & ik\hat{H}_3 & ik\hat{H}_4 \end{array}\right. = \left|\begin{array}{cccc} 1 & 0 & 0 & 0 \\ 0 & 1 & 0 & 0 \\ 0 & 0 & 1 & 0 \\ 0 & 0 & 0 & -ik\overline{K}^{-1} \end{array}\right. = C\ . \tag{23}$$

The matrix A is real and symmetric. As a consequence, its inverse will also be real and symmetric. Using the explicit form of matrix C , we can write the solution to (22) as

$$B = A^{-1} \times C = \begin{bmatrix} A^{-1}_{11} & A^{-1}_{12} & A^{-1}_{13} & -(ik\overline{K}^{-1})A^{-1}_{14} \\ A^{-1}_{21} & A^{-1}_{22} & A^{-1}_{23} & -(ik\overline{K}^{-1})A^{-1}_{24} \\ A^{-1}_{31} & A^{-1}_{32} & A^{-1}_{33} & -(ik\overline{K}^{-1})A^{-1}_{34} \\ A^{-1}_{41} & A^{-1}_{42} & A^{-1}_{43} & -(ik\overline{K}^{-1})A^{-1}_{44} \end{bmatrix}\ . \tag{24}$$

Finally, comparing Eqs. (23) and (24),

$$k^2 \hat{G}_{ij} = A^{-1}_{ij} \quad (i, j = 1,3)\ , \tag{25}$$

$$k^2 \hat{G}_{i4} = -(ik\overline{K}^{-1})A^{-1}_{i4} \quad \Rightarrow \quad (ik\overline{K})\hat{G}_{i4} = A^{-1}_{i4} \quad (i = 1,3)\ , \tag{26}$$

$$ik\hat{H}_i = A^{-1}_{4i} \quad (i = 1,3)\ , \tag{27}$$

$$ik\hat{H}_4 = -(ik\overline{K}^{-1})A^{-1}_{44} \quad \Rightarrow \quad -\overline{K}\,\hat{H}_4 = A^{-1}_{44}\ . \tag{28}$$

Since the components of A are real functions of α_i, so are the components of A^{-1}, and so $k^2\hat{G}_{ij}$ and $ik\hat{H}_i$ are real functions of α_i. This property leads to real integrals in the derivation that follows.

2.3. Integration of Equations—Eshelby Tensors and Eshelby Factors

Now that we have a solution for the Green tensors, we can write the solution of our problem using the convolution integrals (15). The local deviation in velocity is given by

$$\begin{aligned}\tilde{\dot{u}}_k(\bar{x}) &= \int_{R^3} G_{km}(\bar{x}-\bar{x}')\, f_m(\bar{x}')\, d\bar{x}' = \\ &= \int_{R^3} G_{ki}(\bar{x}-\bar{x}')\, f_i^d(\bar{x}')\, d\bar{x}' + \int_{R^3} G_{k4}(\bar{x}-\bar{x}')\, f^s(\bar{x}')\, d\bar{x}' \ .\end{aligned} \tag{29}$$

Taking partial derivatives of Eq. (29), we obtain

$$\tilde{\dot{u}}_{k,l}(\bar{x}) = \tilde{\dot{u}}^d_{k,l}(\bar{x}) + \tilde{\dot{u}}^s_{k,l}(\bar{x}) \ , \tag{30}$$

where the "deviatoric" and "spherical" contributions to the local deviation of velocity gradient field are defined by

$$\tilde{\dot{u}}^d_{k,l}(\bar{x}) = \int_{R^3} G_{ki,l}(\bar{x}-\bar{x}')\, f_i^d(\bar{x}')\, d\bar{x}' \ , \tag{31}$$

$$\tilde{\dot{u}}^s_{k,l}(\bar{x}) = \int_{R^3} G_{k4,l}(\bar{x}-\bar{x}')\, f^s(\bar{x}')\, d\bar{x}' \ . \tag{32}$$

Replacing (8) in (31), recalling that $\partial G_{ij}(\bar{x}-\bar{x}')/\partial\bar{x} = -\partial G_{ij}(\bar{x}-\bar{x}')/\partial\bar{x}'$, integrating by parts, and using the divergence theorem, we obtain

$$\tilde{\dot{u}}^d_{k,l}(\bar{x}) = \int_{R^3} G_{ki,jl}(\bar{x}-\bar{x}')\, \sigma^{d*}_{ij}(\bar{x}')\, d\bar{x}' \ . \tag{33}$$

Equation (33) provides an exact implicit solution to the problem. Such solution requires knowledge of the local dependence of the eigenstress tensor. However, we know from the elastic Eshelby inclusion formalism that if the eigenstrain is uniform over an ellipsoidal domain where the stiffness tensor is uniform, then the stress and the strain are constant over the domain of the

inclusion. The latter suggests to assume a constant eigenstress (a priori unknown) within the volume Ω of the inclusion, and zero outside. This allows us to average the local field (33) over the domain Ω and obtain an average strain rate inside the inclusion of the form

$$\tilde{\dot{u}}^{d}_{k,l} = \left(-\frac{1}{\Omega} \int\int_{\Omega\Omega} G_{ki,jl}(\bar{x} - \bar{x}')\, d\bar{x}\, d\bar{x}' \right) \bar{L}_{ijmn}\, \dot{\varepsilon}^{d*}_{mn} \ , \tag{34}$$

where $\tilde{\dot{u}}^{d}_{k,l}$ and $\dot{\varepsilon}^{d*}_{mn}$ have to be interpreted as average quantities inside the grain. Expressing the Green tensor in terms of the inverse Fourier transform (18b) and taking derivatives, we obtain

$$\begin{aligned} \tilde{\dot{u}}^{d}_{k,l} &= \left(\frac{1}{8\pi^3 \Omega} \int\int_{\Omega\Omega} \int_{R^3} \alpha_j\, \alpha_l \left(k^2 \hat{G}_{ki}(\bar{k}) \right) \exp\left[-i\bar{k}(\bar{x} - \bar{x}') \right] d\bar{k}\, d\bar{x}\, d\bar{x}' \right) \bar{L}_{ijmn}\, \dot{\varepsilon}^{d*}_{mn} \\ &= T^{d}_{klij}\, \bar{L}_{ijmn}\, \dot{\varepsilon}^{d*}_{mn} \ . \end{aligned} \tag{35}$$

Writing $d\bar{k}$ in spherical coordinates $d\bar{k} = k^2 \sin\theta\, dk\, d\theta\, d\varphi$ and using Eq. (25), the deviatoric interaction tensor T^{d}_{klij} can be expressed as

$$T^{d}_{klij} = \frac{1}{8\pi^3 \Omega} \int_0^{2\pi} \int_0^{\pi} \alpha_j\, \alpha_l\, A^{-1}_{ki}(\bar{\alpha})\, \Lambda(\bar{\alpha}) \sin\theta\, d\theta\, d\varphi \ , \tag{36}$$

where θ and φ are the spherical coordinates of the Fourier unit vector $\bar{\alpha}$ and

$$\Lambda(\bar{\alpha}) = \int_0^{\infty} \left(\int\int_{\Omega\Omega} \exp\left[-i\bar{k}(\bar{x} - \bar{x}') \right] d\bar{x}\, d\bar{x}' \right) k^2 dk \ . \tag{37}$$

Integration of Eq. (37) inside an ellipsoidal grain of radii (a, b, c) is given in Appendix A [Eq. (A5)]:

$$\Lambda(\bar{\alpha}) = \frac{8\pi^3}{3} \frac{(abc)^2}{[\rho(\bar{\alpha})]^3} \ , \tag{38}$$

where $\rho(\bar{\alpha}) = \left[(a\alpha_1)^2 + (b\alpha_2)^2 + (c\alpha_3)^2 \right]^{1/2}$. Replacing Eq. (38) in Eq. (36), the expression of T^{d}_{klij} for an ellipsoidal grain is

$$T^{d}_{klij} = \frac{abc}{4\pi}\int_0^{2\pi}\int_0^{\pi} \frac{\alpha_j\,\alpha_l\,A^{-1}_{ki}(\bar{\alpha})}{[\rho(\bar{\alpha})]^3}\sin\theta\,d\theta\,d\varphi \ . \tag{39}$$

Working analogously with Eq. (32), and using Eqs. (9), (18b), and (26), we obtain

$$\begin{aligned}\tilde{\dot{u}}^{s}_{k,l} &= \left(-\frac{1}{\Omega}\int_{\Omega}\int_{\Omega} \bar{K}\,G_{k4,l}(\bar{\mathbf{x}}-\bar{\mathbf{x}}')\,d\bar{x}\,d\bar{x}'\right)\dot{\varepsilon}^{s*} = \\ &= \left(\frac{1}{8\pi^3\Omega}\int_{\Omega}\int_{\Omega}\int_{R^3} \alpha_l\,A^{-1}_{k4}\exp\left[-i\bar{k}(\bar{x}-\bar{x}')\right]d\bar{k}\,d\bar{x}\,d\bar{x}'\right)\dot{\varepsilon}^{s*} = T^{s}_{kl}\,\dot{\varepsilon}^{s*} \ .\end{aligned} \tag{40}$$

After integrating in $d\bar{x}$, $d\bar{x}'$, and dk and using Eq. (38), the spherical Green interaction tensor T^{s}_{kl} for an ellipsoidal grain reduces to

$$T^{s}_{kl} = \frac{abc}{4\pi}\int_0^{2\pi}\int_0^{\pi} \frac{\alpha_l\,A^{-1}_{k4}(\bar{\alpha})}{[\rho(\bar{\alpha})]^3}\sin\theta\,d\theta\,d\varphi \ . \tag{41}$$

Finally, the convolution integral over the Green tensor $\hat{H}(\bar{x})$ allows us to obtain an expression for the mean stress deviation $\tilde{\sigma}^{s}(\bar{x})$, which is the fourth unknown function in differential system (7). Since the latter is not relevant to the present work, its derivation is presented in Appendix B mostly for the sake of completeness. This way of computing the hydrostatic pressure field has been used by Lebensohn et al. (1998) in a particular application of VPSC to make a transition from viscoplastic incompressible loading to elastic unloading.

The expressions (39) and (41) have to be integrated numerically (we use a Gauss-Legendre technique). The evaluation of the integrand requires us to invert the 4×4 linear system (23) for each integration point. For numerical purposes it is convenient to define fourth-order "deviatoric" and second-order "spherical" symmetric Eshelby tensors as

$$S^{d}_{ijkl} = \frac{1}{4}\left(T^{d}_{ijmn} + T^{d}_{jimn} + T^{d}_{ijnm} + T^{d}_{jinm}\right)\bar{L}_{mnkl} \ , \tag{42}$$

$$S^{s}_{ij} = \frac{1}{2}\left(T^{s}_{ij} + T^{s}_{ji}\right) . \tag{43}$$

Replacing (35) and (40) in (30), taking the symmetric component, and using (42) and (43), we obtain the strain-rate deviation in the ellipsoid

$$\tilde{\dot{\varepsilon}}_{ij} = S^{d}_{ijkl}\dot{\varepsilon}^{d*}_{kl} + S^{s}_{ij}\,\dot{\varepsilon}^{s*} \ . \tag{44}$$

The deviator and the trace of $\tilde{\dot{\varepsilon}}_{ij}$ are

$$\tilde{\dot{\varepsilon}}^{d}_{ij} = S^{d}_{ijmn}\dot{\varepsilon}^{d*}_{mn} + S^{s}_{ij}\,\dot{\varepsilon}^{s*} - \frac{1}{3}\delta_{ij}\,\tilde{\dot{\varepsilon}}^{s} \ , \tag{45}$$

$$\tilde{\dot{\varepsilon}}^{s} = S^{d}_{kkmn}\,\dot{\varepsilon}^{d*}_{mn} + \Psi\,\dot{\varepsilon}^{s*} \ , \tag{46}$$

where $\Psi = \mathrm{tr}(S^{s}_{ij})$ will be called in what follows the "spherical Eshelby factor." At this point, we need to find the deviatoric and spherical eigenstrain rates. From Eq. (46), we have

$$\dot{\varepsilon}^{s*} = \frac{\tilde{\dot{\varepsilon}}^{s}}{\Psi} - \frac{S^{d}_{kkmn}}{\Psi}\dot{\varepsilon}^{d*}_{mn} \ . \tag{47}$$

Replacing (47) inside (45),

$$\tilde{\dot{\varepsilon}}^{d}_{ij} = \left(S^{d}_{ijmn} - \xi_{ijmn}\right)\dot{\varepsilon}^{d*}_{mn} + \beta_{ij}\tilde{\dot{\varepsilon}}^{s} \ , \tag{48}$$

where

$$\beta_{ij} = \frac{S^{s}_{ij}}{\mathrm{tr}(S^{s}_{ij})} - \frac{\delta_{ij}}{3} \ , \tag{49a}$$

$$\xi_{ijmn} = \frac{S^{s}_{ij}\,S^{d}_{kkmn}}{\Psi} \ . \tag{49b}$$

According to (48), β_{ij} describes the coupling between the spherical and the deviatoric components of the strain rate. For this reason, it will be called here "the Eshelby coupling tensor." Furthermore, using symmetry considerations, it is easy to realize that (49a) would vanish in the case of a spherical inclusion embedded in an isotropic matrix. As a consequence, β_{ij} can be interpreted as a measure of the anisotropy of the medium, and the deviatoric-spherical coupling can be expected to become stronger as the anisotropy of the medium increases or to

vanish if the medium is isotropic. The latter situation, however, is never found if the material's behavior is nonlinear (i.e., $n \neq 1$ in Eq. 1). In such a case, even if the polycrystal has a random texture, the viscoplastic compliance tensor is a function of the stress state and the response of the homogeneous medium will be, in general, anisotropic, resulting in a nonvanishing β_{ij} tensor. On the other hand, in what concerns ξ_{ijmn}, we have checked numerically (see Appendix C) that the norm of ξ_{ijmn} is, for our purposes, at least two orders of magnitude smaller than the norm of S^{d}_{ijmn} and can be neglected. Then, the following approximation holds:

$$\tilde{\dot{\varepsilon}}^{d}_{ij} \cong S^{d}_{ijmn}\dot{\varepsilon}^{d*}_{mn} + \beta_{ij}\,\tilde{\dot{\varepsilon}}^{s} \ , \tag{50}$$

from where the deviatoric eigenstrain rate $\dot{\varepsilon}^{d*}_{mn}$ is obtained as

$$\dot{\varepsilon}^{d*}_{mn} = S^{d\,-1}_{mnpq}(\tilde{\dot{\varepsilon}}^{d}_{pq} - \beta_{pq}\,\tilde{\dot{\varepsilon}}^{s}) \ . \tag{51}$$

Replacing Eq. (51) in Eq. (47), it can be proved, using $S^{d}_{kkmn}S^{d\,-1}_{mnpq} = \delta_{kp}\delta_{kq}$, $\mathrm{tr}\,\tilde{\dot{\varepsilon}}^{d}_{ij} = 0$, and $\mathrm{tr}\,\beta_{ij} = 0$, that

$$\dot{\varepsilon}^{s*} = \frac{\tilde{\dot{\varepsilon}}^{s}}{\Psi} \ . \tag{52}$$

Equation (51) indicates that the deviatoric strain rate is coupled to both the deviatoric eigenstrain rate and the eigendilatation rate, while (52) shows that, under assumption (50), the dilatation rate depends only on the eigendilatation rate.

2.4. Interaction and Localization Equations

The local constitutive behavior expressed by Eq. (2) also describes the relation between the average stress and strain rate in the domain of the grains, namely,

$$\dot{\varepsilon}^{d}_{ij} = M_{ijkl}\,\sigma^{d}_{kl} + \dot{\varepsilon}^{do}_{ij} \ , \tag{53a}$$

$$\dot{\varepsilon}^{s} = K^{-1}\,\sigma^{s} \ . \tag{53b}$$

For completeness, we copy below Eq. (3), describing the relation between the macroscopic stress and strain rate in the effective medium:

$$\dot{E}^{d}_{ij} = \overline{M}_{ijkl}\,\Sigma^{d}_{kl} + \dot{E}^{do}_{ij}\ , \tag{54a}$$

$$\dot{E}^{s} = \overline{K}^{-1}\,\Sigma^{s}\ . \tag{54b}$$

Expressions similar to Eqs. (5) relating deviations with respect to overall quantities also hold for the average stress, strain rate, and eigenstrain rates in the grains:

$$\tilde{\sigma}^{d}_{ij} = \overline{L}_{ijkl}\left(\tilde{\dot{\varepsilon}}^{d}_{kl} - \dot{\varepsilon}^{d*}_{kl}\right), \tag{55a}$$

$$\tilde{\sigma}^{s} = \overline{K}\left(\tilde{\dot{\varepsilon}}^{s} - \dot{\varepsilon}^{s*}\right). \tag{55b}$$

Replacing the expressions (51) and (52) that give the eigenstrain rates in terms of the strain-rate deviations into the deviation equations (55), we obtain the following interaction equations:

$$\tilde{\dot{\varepsilon}}^{d}_{ij} = -\tilde{M}_{ijkl}\,\tilde{\sigma}^{d}_{kl} - \tilde{\beta}_{kl}\tilde{\sigma}^{s}\ , \tag{56a}$$

$$\tilde{\dot{\varepsilon}}^{s} = -(1/\tilde{K})\,\tilde{\sigma}^{s}\ , \tag{56b}$$

where the interaction tensors and factor are given by

$$\tilde{M}_{ijkl} = \left(I - S^{d}\right)^{-1}_{ijmn} S^{d}_{mnpq}\,\overline{M}_{pqkl}\ , \tag{57a}$$

$$\tilde{\beta}_{ij} = (1/\tilde{K})\left(I - S^{d}\right)^{-1}_{ijmn}\beta_{mn}\ , \tag{57b}$$

$$\tilde{K} = \frac{1-\Psi}{\Psi}\,\overline{K}\ . \tag{57c}$$

Replacing the local and overall deviatoric constitutive relations (53) and (54) into the interaction equations (56), we can write, after some manipulation, the following localization equations for the deviatoric and spherical stress components:

$$\sigma^{d}_{ij} = B_{ijkl}\,\Sigma^{d}_{kl} + \Phi_{ij}\ , \tag{58a}$$

$$\sigma^{s} = B^{s}\,\Sigma^{s}\ , \tag{58b}$$

where the localization tensors are defined as

$$B_{ijkl} = \left(M + \tilde{M}\right)^{-1}_{ijmn}\left(\overline{M} + \tilde{M}\right)_{mnkl}\ , \tag{59a}$$

$$\Phi_{ij} = \left(M + \tilde{M}\right)^{-1}_{ijkl}\left(\dot{E}^{do}_{kl} - \dot{\varepsilon}^{do}_{kl} - \tilde{\beta}_{kl}\tilde{\sigma}^{s}\right), \tag{59b}$$

$$B^s = \frac{K}{\overline{K}} \frac{\overline{K} + \tilde{K}}{K + \tilde{K}} \quad . \tag{59c}$$

For a solid phase ($K \to \infty$) the limit of Eq. (59c) is well defined. However, in the case of a void phase, for which $L_{ijkl} = 0$, $M_{ijkl} \to \infty$, and $K = 0$, the localization tensors become null tensors

$$B_{ijkl} = 0 \ , \ \Phi_{ij} = 0 \ , \ B^s = 0 \ , \tag{60}$$

which is to be expected, since a void cannot sustain stress. However, the void does contribute to strain. As a consequence, we need to derive alternative localization equations in terms of strain rates. Inverting Eqs. (53) and (54) and expressing them in terms of stiffness tensors (i.e., $L_{ijkl} = M^{-1}_{ijkl}$, $\overline{L}_{ijkl} = \overline{M}^{-1}_{ijkl}$ and $\tilde{L}_{ijkl} = \tilde{M}^{-1}_{ijkl}$), and following a similar procedure, we obtain the localization relation for the strain-rate components:

$$\dot{\varepsilon}^d_{ij} = A_{ijkl} \, \dot{E}^d_{kl} + \Omega_{ij} \ , \tag{61a}$$

$$\dot{\varepsilon}^s = A^s \, \dot{E}^s \ . \tag{61b}$$

For the solid phase ($K \to \infty$), the localization tensors are

$$A_{ijkl} = \left(L + \tilde{L}\right)^{-1}_{ijmn} \left(\overline{L} + \tilde{L}\right)_{mnkl} \ , \tag{62a}$$

$$\Omega_{ij} = \left(L + \tilde{L}\right)^{-1}_{ijkl} \left(- \overline{L} : \dot{E}^{do} + L : \dot{\varepsilon}^{do} - \tilde{L} : \tilde{\beta} \, \tilde{\sigma}^s \right)_{kl} \ , \tag{62b}$$

$$A^s = \frac{\overline{K} + \tilde{K}}{K + \tilde{K}} = 0 \ , \tag{62c}$$

while for the void phase ($K = 0$), they are

$$A_{ijkl} = I_{ijkl} + \tilde{L}^{-1}_{ijmn} \, L_{mnkl} \ , \tag{63a}$$

$$\Omega_{ij} = -\tilde{L}^{-1}_{ijkl} \, L_{klmn} \, \dot{E}^{do}_{mn} - \tilde{\beta}_{ij} \, \tilde{\sigma}^s \ , \tag{63b}$$

$$A^s = \frac{\overline{K} + \tilde{K}}{\tilde{K}} \quad . \tag{63c}$$

2.5. Self-Consistent Polycrystal Model

The derivation presented in the previous sections solves the problem of a viscoplastic compressible inclusion embedded in a viscoplastic compressible effective medium being subject to external loading conditions. In this section, we are going to use the previous result to construct a polycrystal model that regards each grain as an ellipsoidal inclusion embedded in an effective medium which represents the polycrystal. The properties of such media are not known a priori but have to be found thorough an iterative self-consistent procedure. Replacing the stress localization Eq. (58) in the local constitutive Eq. (53), we obtain

$$\dot{\varepsilon}_{ij}^{d} = M_{ijkl}\,\sigma_{kl}^{d} + \dot{\varepsilon}_{ij}^{do} = M_{ijkl}\,B_{klmn}\,\Sigma_{mn}^{d} + M_{ijkl}\,\Phi_{kl} + \dot{\varepsilon}_{ij}^{do}\ , \tag{64a}$$

$$\dot{\varepsilon}^{s} = K^{-1}\,\sigma^{s} = K^{-1}\,B^{s}\,\Sigma^{s}\ . \tag{64b}$$

Enforcing the condition that the weighted average of the strain rate over the aggregate has to coincide with the macroscopic quantities, i.e.,

$$\dot{E}_{ij}^{d} = \left\langle \dot{\varepsilon}_{ij}^{d} \right\rangle, \quad \dot{E}^{s} = \left\langle \dot{\varepsilon}^{s} \right\rangle\ , \tag{65}$$

and using the constitutive Eq. (54), we obtain

$$\overline{M}_{ijmn}\,\Sigma_{mn}^{d} + \dot{E}_{ij}^{do} = \left\langle M_{ijkl}\,B_{klmn} \right\rangle \Sigma_{mn}^{d} + \left\langle M_{ijkl}\,\Phi_{kl} + \dot{\varepsilon}_{ij}^{do} \right\rangle\ , \tag{66a}$$

$$\overline{K}^{-1}\,\Sigma^{s} = \left\langle K^{-1}\,B^{s} \right\rangle \Sigma^{s}\ . \tag{66b}$$

Equating the linear and independent terms leads to the following self-consistent equations for the homogeneous compliances and back-extrapolated term,

$$\overline{M}_{ijmn} = \left\langle M_{ijkl}\,B_{klmn} \right\rangle\ , \tag{67a}$$

$$\dot{E}_{ij}^{do} = \left\langle M_{ijkl}\,\Phi_{kl} + \dot{\varepsilon}_{ij}^{do} \right\rangle\ , \tag{67b}$$

$$\overline{K} = \left\langle K^{-1} B^{s} \right\rangle^{-1}\ . \tag{67c}$$

Replacing the strain-rate localization Eq. (61a) in Eq. (64a) and using Eq. (54a) gives

$$A_{ijkl}\,\overline{M}_{klmn}\,\Sigma_{mn}^{d} + A_{ijkl}\,\dot{E}_{kl}^{do} + \Omega_{ij} = M_{ijkl}\,B_{klmn}\,\Sigma_{mn}^{d} + M_{ijkl}\,\Phi_{kl} + \dot{\varepsilon}_{ij}^{do}\ , \tag{68}$$

from where

$$M_{ijkl}\, B_{klmn} = A_{ijkl}\, \overline{M}_{klmn} \ , \tag{69a}$$

$$M_{ijkl}\, \Phi_{kl} + \dot{\varepsilon}^{do}_{ij} = A_{ijkl}\, \dot{E}^{do}_{kl} + \Omega_{ij} \ . \tag{69b}$$

The relations (69) are especially useful when the averages in (67) have to be evaluated for the void phase, in which case $M_{ijkl} \to \infty$, $B_{ijkl} = 0$, and $\Phi_{ij} = 0$.

If the shape of the grains and the voids is the same, then the Eshelby factor Ψ and therefore $\tilde{K}$ [given by Eq. (57c)], are unique. In such a case, Eq. (67c) gives the following self-consistent equation for the effective bulk modulus:

$$\overline{K} = \left\langle \frac{K}{K + \tilde{K}} \right\rangle (\overline{K} + \tilde{K}) \ . \tag{70}$$

Since $K \to \infty$ for the incompressible material phase and $K = 0$ for the void phase, it holds that

$$\frac{K}{K + \tilde{K}} = \begin{Bmatrix} 1 & \text{for grains} \\ 0 & \text{for voids} \end{Bmatrix} . \tag{71}$$

Then the self-consistent equation for the viscoplastic bulk modulus is given by

$$\overline{K} = \frac{1 - \phi}{\Psi}\, \overline{K} \ , \tag{72}$$

where ϕ is the current porosity (relative volume fraction of voids) in the polycrystal.

The self-consistent equations (67), are derived imposing the average of the local strain rates to coincide with the applied macroscopic strain rate [Eq. (65)]. It can be shown (see Appendix D) that these equations are also consistent with the condition that the average of the local stresses coincides with the macroscopic stress only if the shape of all inclusions (grains and voids) is unique. If the grains and the voids each have a different shape, they have associated different Eshelby tensors and factors, and consequently the interaction tensors cannot be factored from the averages. In this case, the following general self-consistent expressions (derived in Appendix D) should be used (Walpole, 1969; Lebensohn et al., 1996):

$$\overline{M}_{ijkl} = \left\langle M : B \right\rangle_{ijmn} \left\langle B \right\rangle^{-1}_{mnkl} \ , \tag{73a}$$

$$\dot{E}^{do}_{ij} = \left\langle M : \Phi + \dot{\varepsilon}^{do} \right\rangle_{ij} - \left\langle M : B \right\rangle_{ijkl} \left\langle B \right\rangle^{-1}_{klmn} \left\langle \Phi \right\rangle_{mn} \ , \tag{73b}$$

$$\overline{K} = \frac{1-\phi}{\phi} \ \frac{1-\Psi_v}{\Psi g} \overline{K} \ , \tag{73c}$$

Ψ_g and Ψ_v the trace of the spherical Eshelby tensors associated with the grains and the voids, respectively. In writing Eq. (73c), we assume that all the grains have a similar shape and all the voids have the a similar shape.

The self-consistent Eqs. (67) are a particular case of Eqs. (73). Both sets constitute fixed-point equations that provide improved estimates of $\overline{M}_{ijkl}$, $\dot{E}^{do}_{ij}$, and $\overline{K}$ when they are solved iteratively starting from an initial guess for the latter tensors. From a numerical point of view, Eqs. (73) are more robust and improve the speed and stability of the convergence procedure even when solving a problem where all the inclusions have the same shape.

2.6. Local Linearization for Voided Polycrystals

As stated earlier, the deviatoric local constitutive behavior [Eq. (2a)] can be linearized in different ways, and the macroscopic response resulting from the self-consistent formulation will depend on the choice made for that linearization. For instance, if the back-extrapolated term $\dot{\varepsilon}^{do}_{ij}$ is a priori set to zero, the resulting model is a secant one, which has been proved to be, in general, too stiff, leading to close-to-upper-bound results. On the other hand, if $M_{ijkl} = \partial \dot{\varepsilon}^{d}_{ij}\left(\sigma^{d}_{ij}\right) / \partial \sigma^{d}_{kl}$, the model is tangent (Molinari et al., 1987; Lebensohn and Tomé, 1993) and gives a more compliant response. However, as pointed out by Ponte Castañeda (2002a), any homogenization scheme whose local linearization depends only on the average of local states in the phases (or grains) fails in reproducing Gurson's results at high triaxialities and leads to a completely rigid response in the pure hydrostatic limit. This result is connected to the high deformation gradients that physically exist inside the phases (or grains) in the vicinity of a void when high hydrostatic pressure is applied to the aggregate. Linearizing a power law using the tangent at the midpoint (first-order moment) of the intragranular stress distribution underestimates, in general, all the rates within the interval. But, in particular, the rates at the

higher stresses that make the effective response of the phases (grains) softer can be seriously underestimated. In fact, Suquet (1995) showed that estimating the magnitudes of the intraphase (intragranular) fluctuations (second-order moments) and linearizing the local behavior in terms of them, rather than just using the average states, softens the predicted effective behavior of the aggregate. For these reasons, good agreement between the present theory (in its isotropic and rate-insensitive limit) and the Gurson model at high triaxialities requires us to generalize the linearization and to formulate a super-tangent approach. We define the slope of the local compliance as

$$M_{ijkl}\left(\hat{\sigma}^{d}_{kl}-\sigma^{d}_{kl}\right)=\left(\hat{\dot{\varepsilon}}^{d}_{ij}-\dot{\varepsilon}^{d}_{ij}\right). \tag{74}$$

Here, σ^{d}_{kl} is the average stress in the grain and $\left(\hat{\sigma}^{d}_{kl}-\sigma^{d}_{kl}\right)$ can be interpreted as a measure of the intragranular stress fluctuation. We propose for $\hat{\sigma}^{d}_{kl}$ an empirical functional form colinear with σ^{d}_{kl}:

$$\hat{\sigma}^{d}_{kl}=\left(1+\alpha(X,\phi)\,|X|\right)\sigma^{d}_{kl}\ . \tag{75}$$

Here, $X=\Sigma^{s}/\Sigma^{d}$ is the stress triaxiality (to be called triaxiality in what follows), Σ^{s} is the macroscopic hydrostatic pressure, $\Sigma^{d}=\left(\tfrac{3}{2}\Sigma^{d}_{ij}\Sigma^{d}_{ij}\right)^{1/2}$ is the macroscopic equivalent deviatoric (Von Mises) stress, and $\alpha(X,\phi)$ is an empirical parameter whose dependence with X and ϕ is adjusted to match the predictions of Gurson's formulation for an isotropic and rate-insensitive polycrystal. Defined in this way, the local tensors $\hat{\sigma}^{d}_{kl}$ are evidently related with the stress fluctuations. Here, rather than estimate them directly, we fit the parameter $\alpha(X,\phi)$ to the Gurson model for different triaxialities and porosities. Observe that by setting $\alpha=0$, the tangent formulation is recovered, while $\alpha<0$ corresponds to a stiffer sub-tangent approximation closer to the secant response.

2.7. Fitting of $\alpha(X,\phi)$ using the Gurson Model

The Gurson (1977) model follows from solving the localization problem on a representative volume element formed by the solid phase and a void included at the center. The assumptions of

the model are that the solid phase is isotropic rigid plastic (with an effective yield stress Y) and rate insensitive, and that the void is spherical. Under such conditions the effective yield stress for the effective medium is

$$\Sigma^{d} = Y\sqrt{1+\phi^{2}-2\phi\cosh\left(\frac{3\Sigma^{s}}{2Y}\right)} \ . \tag{76}$$

Equation (76) describes a yield surface in the 3-D space defined by the normalized stresses Σ^{d}/Y, Σ^{s}/Y and the porosity ϕ. Such a yield surface defines, for a given porosity, the stress state that fulfills the yield condition. This equation depends on the hydrostatic pressure and reduces to the classical Von Mises yield condition when the porosity is null. When the spherical stress component is zero, Eq. (76) predicts a yield stress corrected for the porosity, i.e.,

$$\Sigma^{d} = Y(1-\phi) \ . \tag{77}$$

When the deviatoric stress component is zero, this expression leads to the Carroll and Holt (1972) limit

$$\Sigma^{s} = \tfrac{2}{3} Y \ln\left(1/\phi\right) \ . \tag{78}$$

Equation (78) gives, for a fixed porosity, the value of hydrostatic stress that will produce dilatational plastic deformation. The present viscoplastic formulation cannot be used in the purely hydrostatic limit without encountering mathematical singularities. Such a case, however, can still be treated approximately in the limit of high triaxialities when the hydrostatic component is much larger than the deviatoric one. In what follows, we will fit the parameter $\alpha(X,\phi)$ by matching the result of the self-consistent formulation to the Gurson equation (76) for aggregates with the lowest possible anisotropy and rate sensitivity. For this fitting procedure, the VPSC model has been applied to a fcc aggregate, with 500 randomly oriented spherical grains deforming by (111)<110> slip, containing spherical voids, and using a rate-sensitivity exponent n = 20 considered in what follows as the "rate-insensitive limit." The loading conditions chosen for the fitting correspond to an axisymmetric tensile stress with the transverse stress components being adjusted to keep the triaxiality constant throughout deformation.

In the case of a rate-dependent material, a "yield stress" cannot be defined unambiguously because any nonzero stress state will induce a strain rate. Therefore, if the yield surface of a rate-independent material (such as Gurson's yield surface) is assumed to follow from a plastic potential, it should be compared to a surface of equal dissipation rate of the rate-dependent material. Evidently, the locus of an equal-dissipation-rate surface will depend on the reference dissipation rate chosen. We show in Appendix E that the dissipation rate obtained with VPSC is a homogeneous function of degree (n+1) of the stress. As a consequence, all the equal-dissipation-rate surfaces are homothetic (same shape) and a unique surface is obtained after normalization. In this work, we use as our normalization stress the equivalent stress Σ^d induced by a tensile imposed strain rate of unit norm in a material without voids. The locus of the equal dissipation rate defined by the normalized deviatoric stress, the normalized hydrostatic stress, and the porosity can be directly compared with the rate-independent Gurson yield surface. By adjusting the value of α for parametric values of porosity and triaxiality, the stress predicted by VPSC is made to reproduce the stress state given by the Gurson criterion [Eq. (76)].

Figure 1a (solid lines) shows 2-D sections of the normalized Gurson yield surfaces for different porosities, together with several points of the normalized equal-dissipation-rate surfaces obtained with VPSC for different positive triaxialities using the value of α that optimizes the match with the Gurson surface. The higher the void concentration or the imposed hydrostatic state (i.e., the higher local fluctuations inside a grain), the higher the value of α (i.e., the softer effective behavior of the grain). Figure 1b shows parametric curves of α versus porosity for fixed triaxiality and vice versa. For the sake of completeness, although the above fitting was for tensile states, using symmetry arguments it is easy to prove that $\alpha(X,\phi) = \alpha(|X|,\phi)$ for compressive states ($\Sigma^s < 0 \Rightarrow X < 0$). Concerning the computational implementation of the model, the above information has been used to build an interpolation table that gives α as a function of the current porosity and triaxiality.

The adjustment of α above is performed by matching the VPSC stress to the Gurson stress under the condition of equal dissipation rate. No constraint is imposed on the associated strain rate. Within the Gurson criterion, the latter follows from invoking the associated flow rule (also called the normality rule), which is a common assumption in continuum plasticity theory.

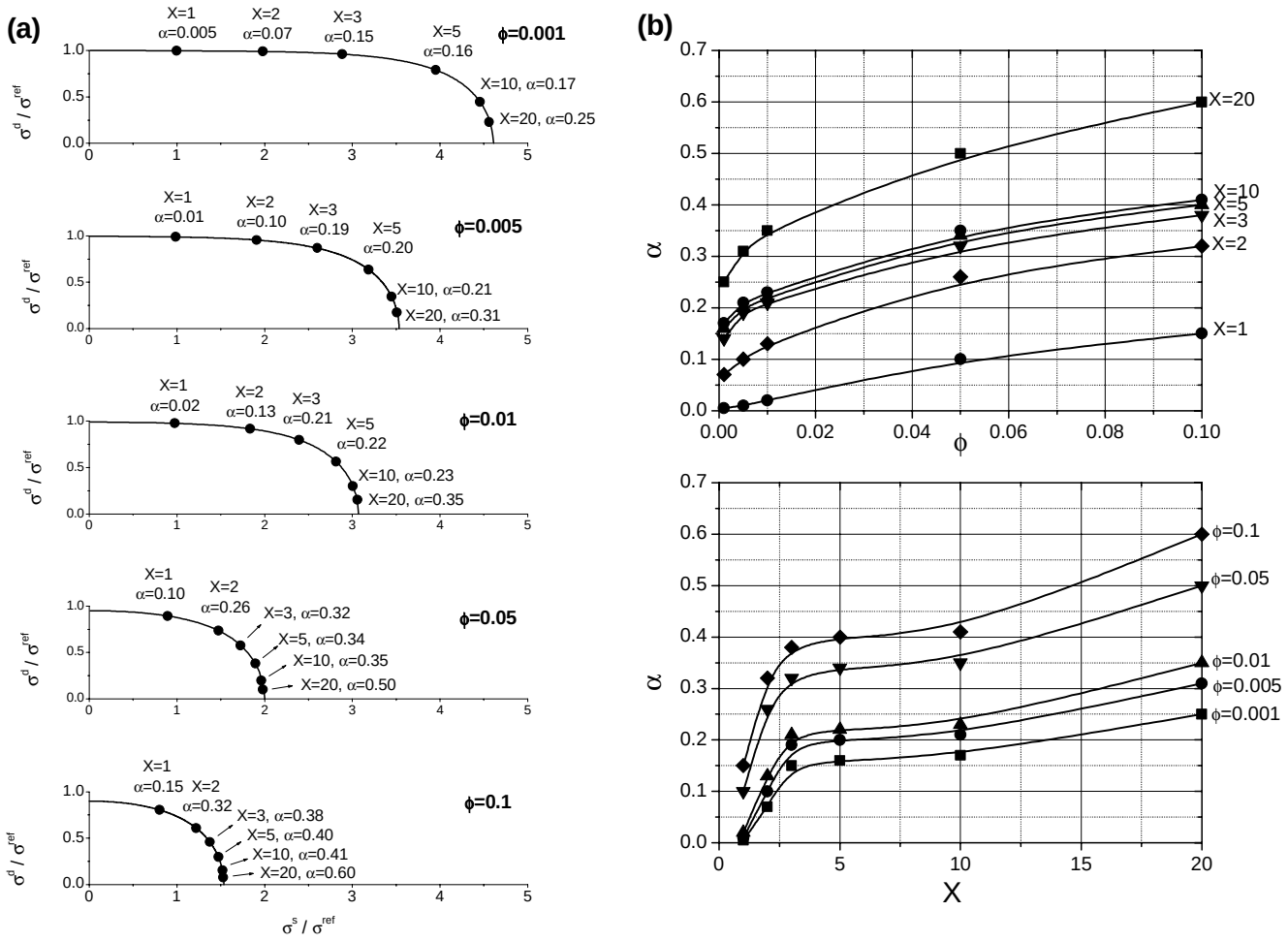

Figure 1. (a) Normalized Gurson yield surface (solid lines) for porosities 0.1%, 0.5%, 1%, 5%, and 10% and points of the normalized equal-dissipation-rate surface for same porosities and triaxialities 0, 1, 2, 3, 5, 10, and 20, calculated with VPSC for the displayed value of the super-tangent parameter α, for the case of a fcc-voided polycrystal, with random crystallographic texture, spherical grains and voids, and viscoplastic exponent n = 20. (b) Dependence of α as a function of porosity for parametric triaxialities and vice versa.

Within the viscoplastic polycrystal approach, however, the strain rate follows from the calculation and is not assumed to be given by the normality rule. Our calculation shows that in our model, the coincidence of the plastic potential and the yield surface is only approximate and becomes more nonassociative with increasing porosity and triaxiality. Figure 2 (left column) shows polar charts displaying the relative deviation between VPSC and Gurson's strain triaxiality at different stress-triaxialities, for two different porosities. This difference in the strain triaxiality predicted by both models can be interpreted into angular deviations of VPSC strain

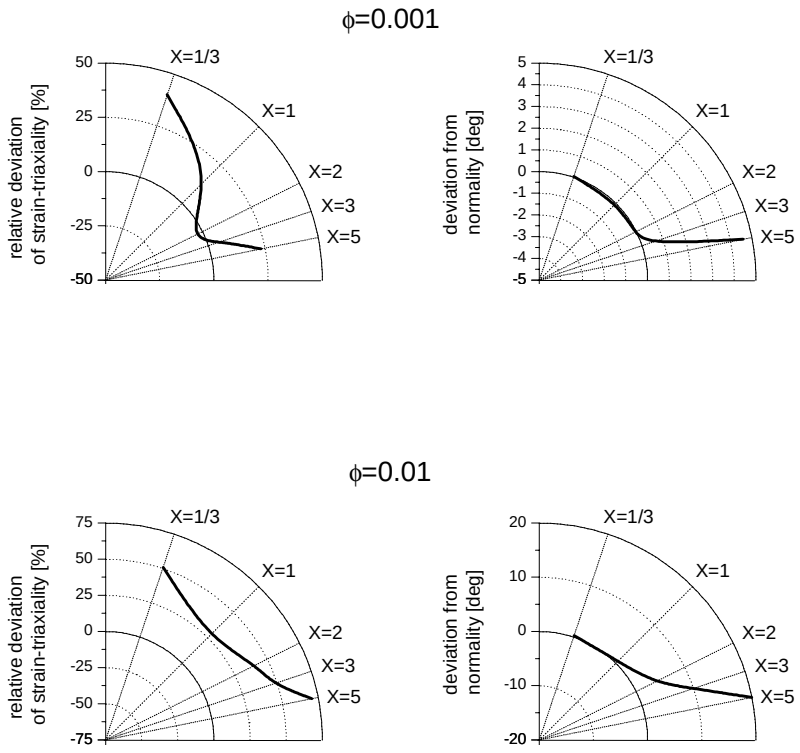

Figure 2. (Left) Polar charts of the relative deviation of VPSC from Gurson's strain triaxiality at different stress triaxialities, for porosities 0.1% and 1%. (Right) Deviations of VPSC strain rates from normality (as assumed by Gurson's model) at different stress triaxialities for porosities 0.1% and 1%.

rates from the normal to the yield surface,[§] and is shown in the plots on the right of Fig. 2. At 0.1% porosity we see that, moving from low- to high-stress triaxialities, VPSC overestimates Gurson's strain triaxialities. This disagreement determines deviations of VPSC from the normality condition, which starts becoming noticeable for triaxialities higher than 3. At a higher porosity (1%), VPSC overestimates Gurson's strain triaxialities by about 25 to 50%, for the whole range of triaxialities considered. This determines a deviation from normality which is close to 20° when X = 5 and is even higher for higher triaxilities.

This result points to the fact that the associated flow rule, which is a valid assumption for describing the constitutive response of solid aggregates, does not apply to voided aggregates.

[§] The axes used for plotting sections of the Gurson yield surface in Fig. 1 introduce a distortion. As a consequence, the components of the vector normal to such surfaces do not coincide with the strain-rate components given by the associative rule and used to compare with VPSC. The rate components associated with Gurson are calculated analytically.

2.8. Numerical Implementation

To illustrate the use of this formulation, we describe here the steps required to predict the rate of porosity evolution $\dot{\phi}$ for a given stress state Σ_{ij} applied to a polycrystal with an initial porosity ϕ. From Σ_{ij} we can derive the mean stress Σ^s, the stress deviator Σ^d_{ij}, the equivalent deviatoric stress Σ^d, and the triaxiality X. With ϕ and X, the value of the super-tangent parameter α can be obtained. In order to start an iterative search of the local states, one should assume initial input values for the local deviatoric stresses and moduli. Taking $\sigma^d_{ij} = \Sigma^d_{ij}$ and using Eqs. (1), (53a), and (74), an initial guess for $\dot{\varepsilon}^d_{ij}$, M_{ijkl}, and $\dot{\varepsilon}^{do}_{ij}$ is obtained for each grain. Next, initial guesses for the macroscopic moduli $\overline{M}_{ijkl}$, $\dot{E}^{do}_{ij}$, and $\overline{K}$ (usually simple averages of the corresponding local moduli) are needed. With these guesses and the applied state Σ_{ij}, the guess for the macroscopic strain rate follows from the constitutive law [Eq. (54)], and the Eshelby tensors and factors S^d_{ijmn}, S^s_{ij}, Ψ, and β^s_{ij} are calculated using the macroscopic moduli plus the grain and void shape by means of the procedure described in Sections 2.2 and 2.3. Subsequently, the interaction tensors and factors $\tilde{\mathbf{M}}_{ijkl}$, $\tilde{\beta}_{ij}$, and $\tilde{K}$ [Eq. (57)] and the localization tensors B_{ijkl}, Φ_{ij}, B^s, A_{ijkl}, Ω_{ij}, and A^s [Eqs. (59) and (62)], can be obtained as well. With these tensors, new estimates of $\overline{M}_{ijkl}$, $\dot{E}^{do}_{ij}$, and $\overline{K}$ are obtained by means of the self-consistent Eqs. (73). After achieving convergence on the macroscopic moduli (and, consequently, also on the macroscopic strain rate and the interaction tensors and factors), new estimates of the local stresses can be obtained using the interaction Eqs. (56). If the recalculated local stresses are different from the input values, a new iteration should be started. If, instead, they coincide within a certain tolerance, the converged value of the macroscopic bulk modulus $\overline{K}$ is used to obtain the macroscopic dilatation rate as $\dot{E}^s = \Sigma^s / \overline{K}$. Finally, the porosity rate is calculated by means of the following kinematic relation (Tveergard, 1981):

$$\dot{\phi} = (1-\phi)\,\dot{E}^s \quad . \tag{79}$$

3. RESULTS

In this section, we present several calculations that illustrate the capabilities of the extended VPSC formulation and compare its predictions with the ones obtained using the classical Gurson's model. We show in what follows how this formulation accounts not only for porosity evolution but also for void shape effects in the mechanical response and in the porosity evolution. The effect of rate sensitivity, texture, and triaxiality upon the mechanical response of a voided material is also investigated in this section.

3.1. Comparison with Gurson for Evolving Porosity

In Section 2.6, we fit the parameter α, i.e., the single adjustable parameter in the present extended VPSC formulation, to match Gurson's results at fixed porosities, for the case of a random fcc polycrystal with spherical voids. Here, we present a comparison of VPSC and Gurson for the case of the same polycrystal, allowing for porosity evolution. In doing so, we minimize the rate effects (taking n = 20, considered to be the rate-insensitive limit) and switch off the microstructure evolution in VPSC (i.e., texture, grain shape, and void shape), except for the porosity evolution. The procedure for this comparison is as follows:

a) Assume a general axisymmetric tensile stress Σ_{ij}, which can always be expressed in terms of the hydrostatic and deviatoric components as $\Sigma_{11} = \Sigma_{22} = \Sigma^s - \frac{1}{3}\Sigma^d$ and $\Sigma_{33} = \Sigma^s + \frac{2}{3}\Sigma^d$.

b) The hydrostatic component Σ^s and a reference flow stress for the solid material Y are kept fixed throughout the calculation. For Σ^s/Y fixed and for a given porosity ϕ_0, the deviatoric equivalent stress Σ^d is obtained from Gurson's Eq. (76). The value of Σ^d is going to evolve with porosity and also with the triaxiality X.

c) Given Σ^s and Σ^d, calculate the triaxiality X and use $\alpha(X,\phi)$ inside VPSC to get $\dot{E}^d = \left(\frac{2}{3}\dot{E}^d_{ij}\dot{E}^d_{ij}\right)^{1/2}$, $\dot{E}^s$, and $\dot{\phi} = (1-\phi_o)\dot{E}^s$.

d) For an imposed deviatoric strain increment ΔE^d, get the time increment $\Delta t = \frac{\Delta E^d}{\dot{E}^d}$ and update the porosity according to (a) Gurson: $\phi = \frac{\phi_o Z}{1-\phi_o+\phi_o Z}$ with $Z = \exp\left(\frac{\sinh\left(3\Sigma^s/2Y\right)}{2\Sigma^d/3Y}\Delta E^d\right)$ (Johnson and Addessio, 1988), and (b) VPSC: $\phi = \phi_o + \dot{\phi}\Delta t$.

Figure 3 shows the porosity evolution as a function of tensile strain for parametric values of Σ^S/Y, as predicted by Gurson and VPSC models. In all cases, the initial porosity was set to 3×10^{-4}. For ratios 1/3 and 1, the total longitudinal strain was evolved to a value of 1. For higher ratios of the parameter, the porosity evolves faster and the Carroll-Holt (1972) limit (Eq. 78) is reached before the final strain is achieved. Although both models exhibit similar trends, there are some quantitative discrepancies (VPSC overestimates the porosity rate with respect to Gurson for values of Σ^S/Y=1/3, 1 and underestimates them for Σ^S/Y=2, 3) which are to be expected since, as shown in Fig. 2, the strain triaxialities which determine the porosity evolution differ from one model to the other. Finally, a numerical aspect of these simulations that should be highlighted is that the VPSC code still converges in the vicinity of the numerically demanding Carroll-Holt limit (i.e., at high triaxialities), although it cannot handle pure hydrostatic conditions.

3.2. Effect of Rate Sensitivity

Another interesting characteristic of the present formulation is that its results depend on the rate sensitivity of the material. This feature can be easily visualized by plotting normalized equal-dissipation-rate surfaces corresponding to different rate-sensitivity exponents. Figure 4 shows these surfaces for 0.5%, 1%, and 5% porosity calculated with VPSC for a random polycrystal with spherical voids, using rate-sensitivity exponents n = 1, n = 3, n = 5, and n = 20 (defined here as the rate-insensitive limit). Even though the associated flow rule does not apply, it is still true that the normal to the equal dissipation surface gives a qualitative estimate of the strain-rate triaxiality (see discussion above). An inspection of the surfaces in Fig. 4 indicates that

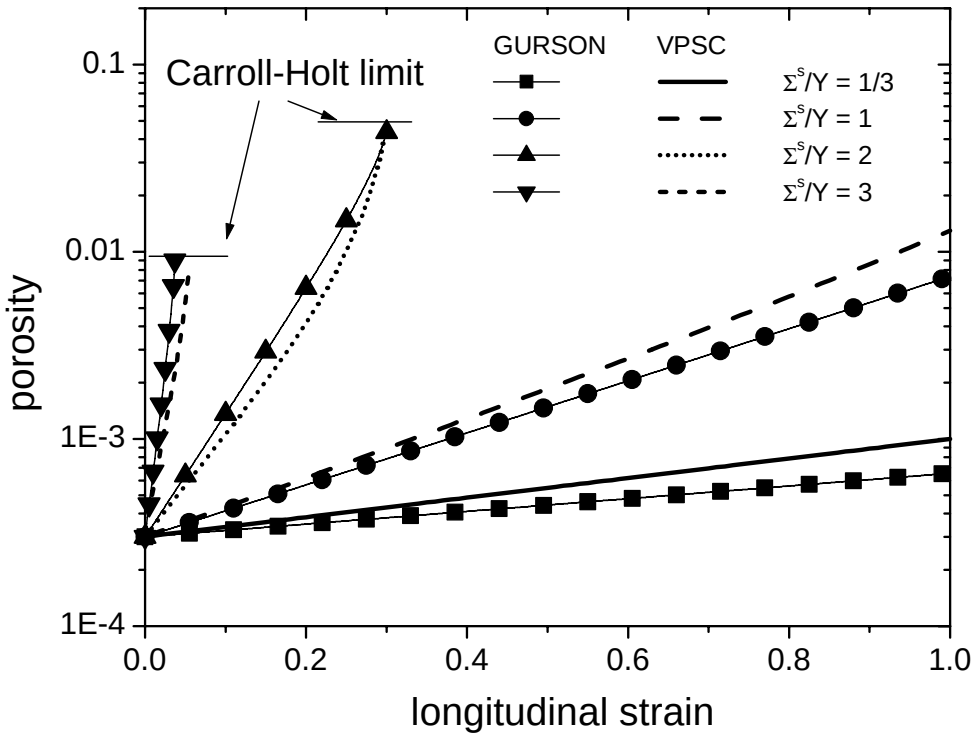

Figure 3. Porosity evolution in an isotropic material (random polycrystal) with spherical voids, deformed in tension, for different triaxialities, as predicted by Gurson (symbols) and VPSC (lines) models. Initial porosity: 3×10^{-4}. Total longitudinal strain: 1.0, for $\Sigma^S / Y = 1/3$ and 1. In the cases of $\Sigma^S / Y = 2$ and 3, the longitudinal strain was limited by the Carroll and Holt condition. No texture or morphology evolution allowed in VPSC cases.

a) At a given porosity and for fixed stress triaxiality (straight line through the origin), the higher the rate sensitivity (lower exponent), the smaller the dilatation component $\dot{E}^s$, and, as a consequence, the lower the required strain triaxiality (defined as $\dot{E}^s / \dot{E}^d$). In other words, the porosity evolution (dilatation rate) will be slower for the same stress triaxiality because the solid phase contributes more to overall deformation as the rate sensitivity of the material increases.

b) As the porosity increases, the relative difference between the surfaces corresponding to different rate sensitivities decreases. In other words, the material becomes less rate sensitive as porosity increases because the cavities themselves are, essentially, rate-insensitive domains. The same tendency was reported by Liu et al. (2002) using a rate-sensitivity extension of the Gurson model.

What the equal-dissipation-rate plots in Fig. 4 show for fixed porosities and different triaxialities can also be shown for a fixed triaxiality and evolving porosity. In Fig. 5, we plot the porosity evolution of a random fcc polycrystal with 1% initial volume fraction of spherical voids for different values of the rate-sensitivity exponent and a fixed traxiality of 1. Evidently, the present model predicts a faster porosity evolution as the rate sensitivity of the solid material decreases.

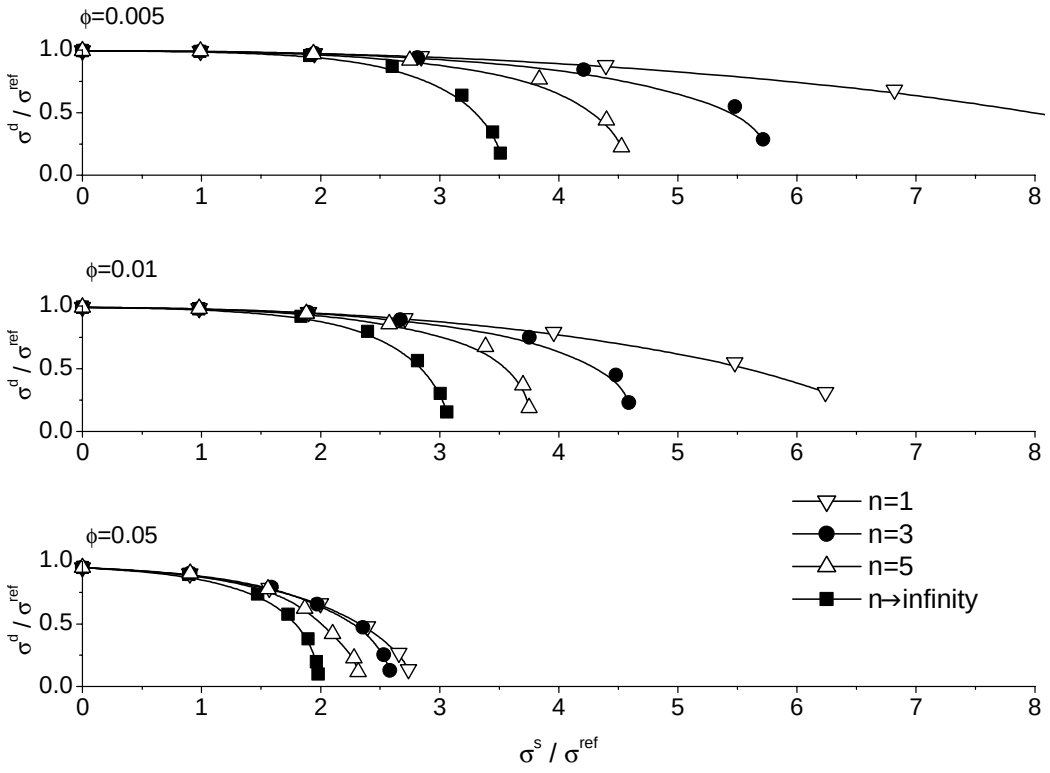

Figure 4. Effect of rate sensitivity. Normalized equal-dissipation-rate surfaces for porosities 0.5%, 1%, and 5%, calculated with VPSC for a random fcc polycrystal with spherical voids for different rate-sensitivity exponents.

3.3. Creep Test Simulation

Fixing the equivalent stress Σ^d and the triaxiality $X = \Sigma^s / \Sigma^d$ and assuming an axisymmetric stress state amounts to prescribing the full stress tensor Σ_{ij} to simulate an axisymmetric triaxial creep test. This case differs from the cases in Section 3.1 where Σ^d is not allowed to evolve. In what follows, we will use such loading conditions to illustrate different anisotropic features of the generalized VPSC model. For this reason, the results are discussed here in some detail.

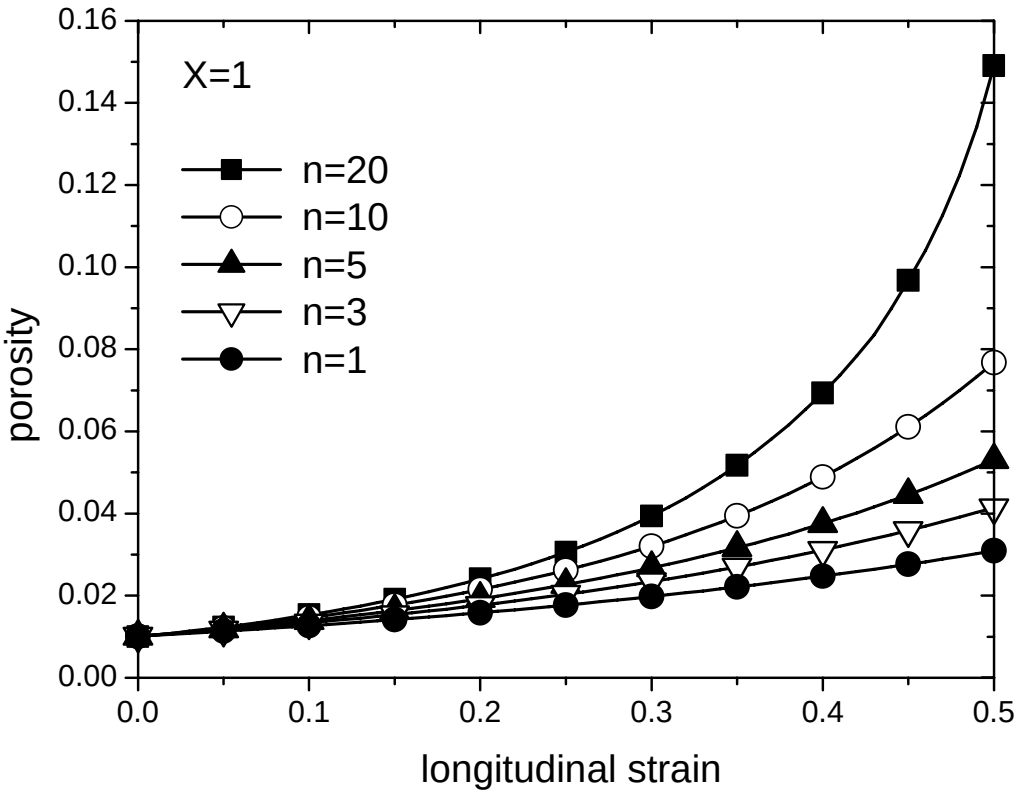

Figure 5. Effect of rate sensitivity. Porosity evolution in a random polycrystal with spherical voids deformed in tension for X = 1 and different rate-sensitivity exponents. Initial porosity 1%. Total longitudinal strain 0.5.

Figure 6 shows the results of a creep test simulation for the case of a random fcc polycrystal containing spherical voids deforming by (111)<110> slip ($\tau^s = 100\,\text{MPa}$), with a rate-sensitivity exponent n = 10 and an initial porosity of 3×10^{-4} under a constant triaxiality of X = 2 and $\Sigma^d = 273$ MPa. No texture development or void-shape evolution was allowed, only void dilatation was accounted for. The porosity evolution (Fig. 6a) shows in a semi-logarithmic representation an initial constant slope until about 5% porosity is reached, followed by an acceleration at high porosities. Note that in this case, the calculation was carried out up to 30% porosity in order to stay below the percolation limit (about 50% porosity), at which point the self-consistent approach fails. Fig. 6b shows that for a constant applied stress, there is a steady increment of the strain-rate components as deformation evolves. This response reflects a softening of the material as porosity increases. These strain-rate increments are higher in the dilatational component than in the deviatoric component. The stress and strain triaxialities,

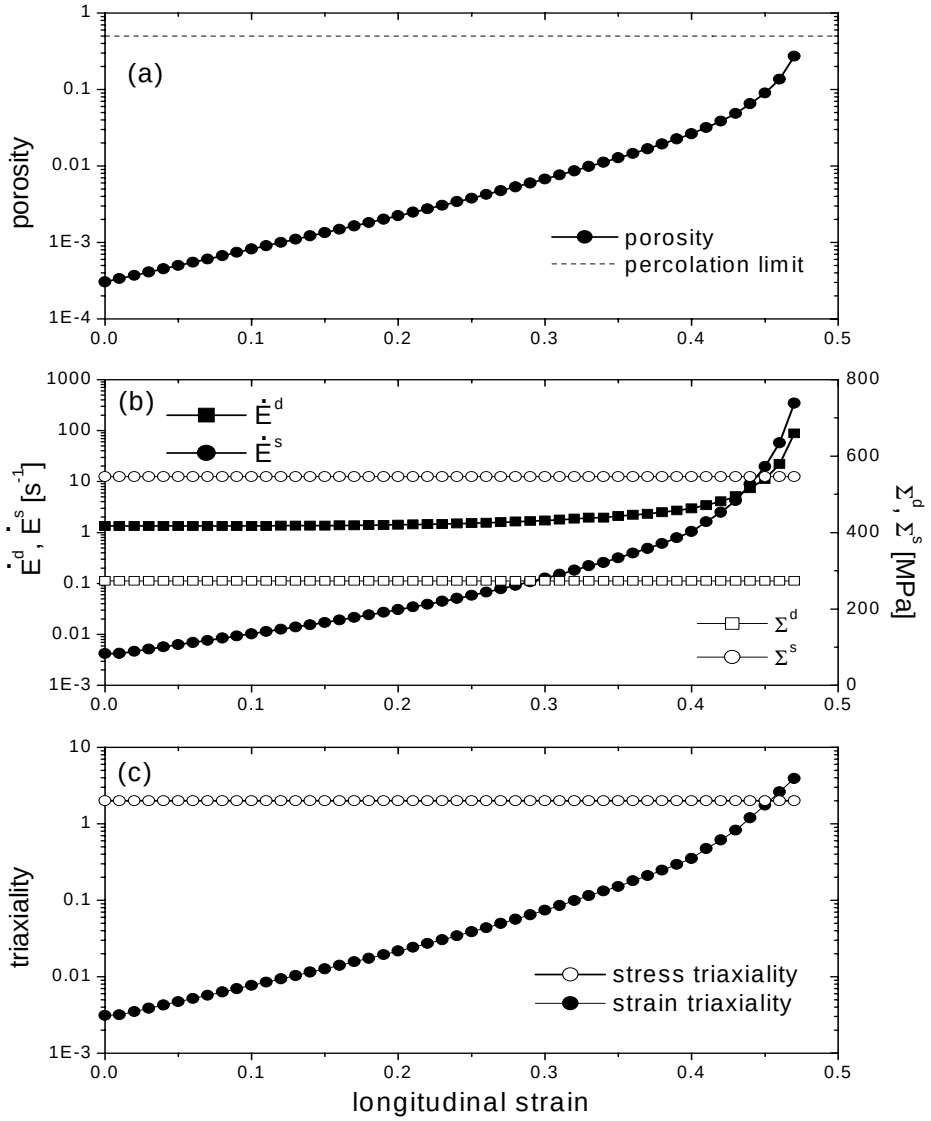

Figure 6. Creep test simulation. Case of a random fcc polycrystal deforming by (111)<110> slip ($\tau^s = 100\,\text{MPa}$)*, n = 10, initial porosity 3 ×10^{-4}, X = 2,* $\Sigma^e = 273\,\text{MPa}$ *, no texture or morphology evolution allowed. (a) Porosity evolution, (b) Deviatoric and spherical components of stress and strain rate, (c) Stress and strain triaxialities.*

plotted in Fig. 6c, reflect the evolution of the individual components. It is worth noting that unlike the rate-insensitive Gurson model that prescribes precise values of flow stress for a given porosity and triaxiality, within the VPSC formulation any imposed stress induces plastic deformation, and the strain rate is determined by the magnitude of the stress components and the current porosity of the material. In the present case of constant stress, for instance, the increase in

porosity accelerates the deformation rate by several orders of magnitude with respect to the initial value.

3.4. Effect of Void Morphology

In order to isolate the effects of void morphology from the full anisotropy evolution due to morphologic and crystallographic texture development, Fig. 7 shows the VPSC predictions of porosity evolution during a creep test for a random fcc polycrystal with different void shapes (spherical, oblate, and prolate) and for triaxialities X = 1/3 (uniaxial stress) and X = 1. In the oblate and prolate case, the short and long axis of the ellipsoidal void, respectively, is aligned with the tensile axis. In all cases, the rate sensitivity exponent is n = 10, initial porosity is 0.5%, the total longitudinal strain imposed is 0.5, and neither texture development nor void morphology evolution were allowed. Note that scales are different since, as expected, porosity increases faster at the higher triaxiality. Oblate voids (axes ratios 5:5:1) tend to grow significantly faster than prolate ones (axes ratios 1:1:5), independent of the triaxiality. This intuitively correct result has also been reported by other authors using different approaches (Lee and Mear, 1992; Ponte Castañeda et al., 1994). Under the present model, the void morphology enters naturally into the formulation via the Eshelby tensor, whose components depend on the orientation and the shape of the cavities present in the material (see Section 2.3).

In addition, it is possible to treat both aligned or arbitrarily distributed void shapes. In the former case, the Eshelby tensor is the same for all the voids, while the latter case requires calculating the Eshelby tensor for each void, which results in a more time-consuming calculation.

3.5. Coupling between Texture Development and Porosity Evolution

The present model allows us to account for the anisotropic response of voided polycrystals induced by the development of crystallographic or morphologic textures. While the former is due to crystal rotations associated with plastic distortion of the grains, the latter refers to changes in the shape of both voids and grains. Figure 8(a) shows the porosity evolution in an fcc polycrystal with initially random crystallographic texture, a rate-sensitivity exponent of n = 10, an initial porosity of 1%, for a simulation of an axisymmetric creep test with a triaxiality X = 1 and a total longitudinal strain of 0.5. The different cases are for voids of different initial shapes (spherical or prolate with a long-to-short ratio of 5) with or without texture evolution. When no

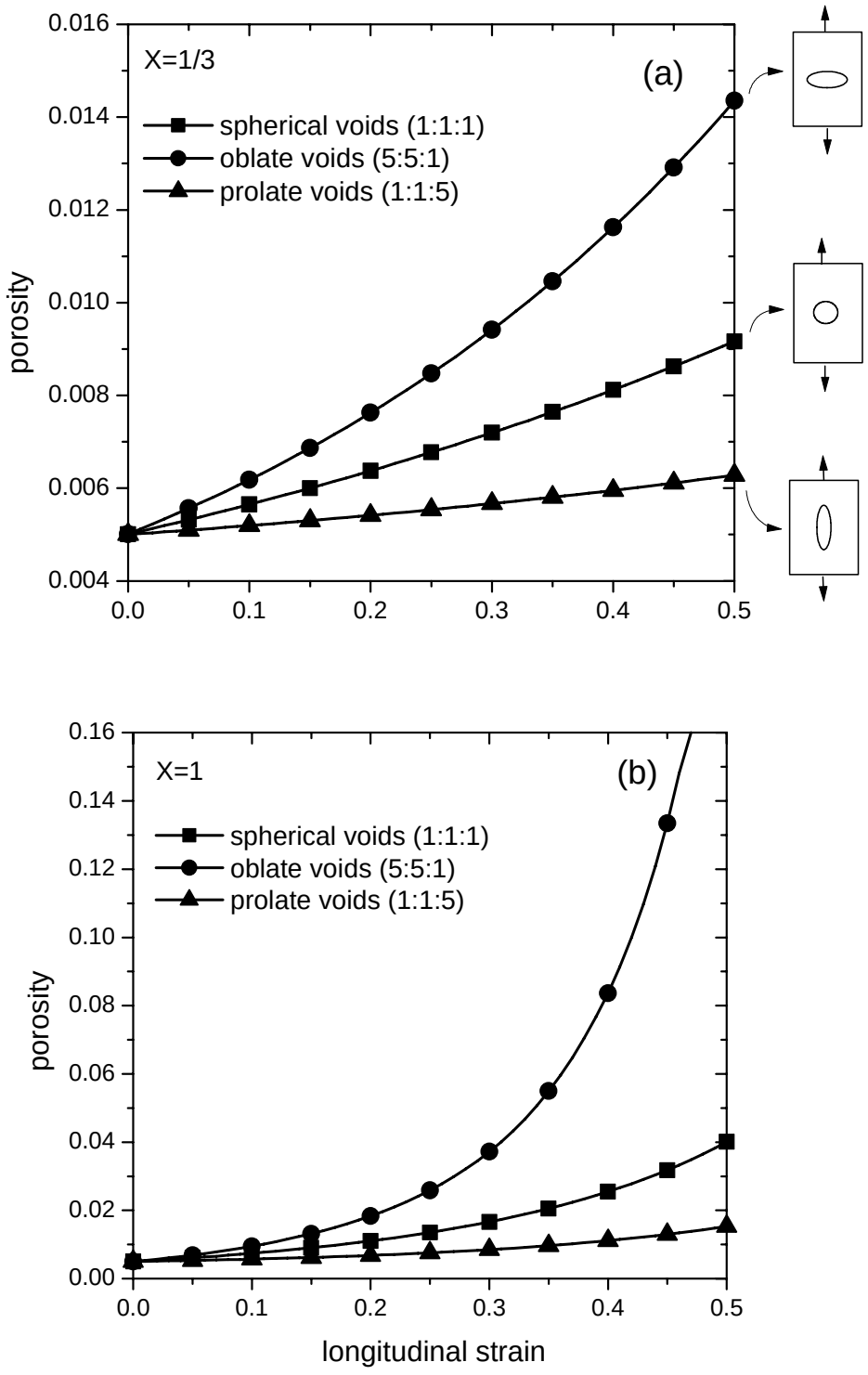

Figure 7. Effect of void shape. VPSC predictions of porosity evolution during a creep test performed on an fcc polycrystal with random texture for different void morphologies, with no texture or morphology evolution. Initial porosity 0.5%, n = 10, total longitudinal strain 0.5. Cases of (a) triaxiality = 1/3, (b) triaxiality = 1.

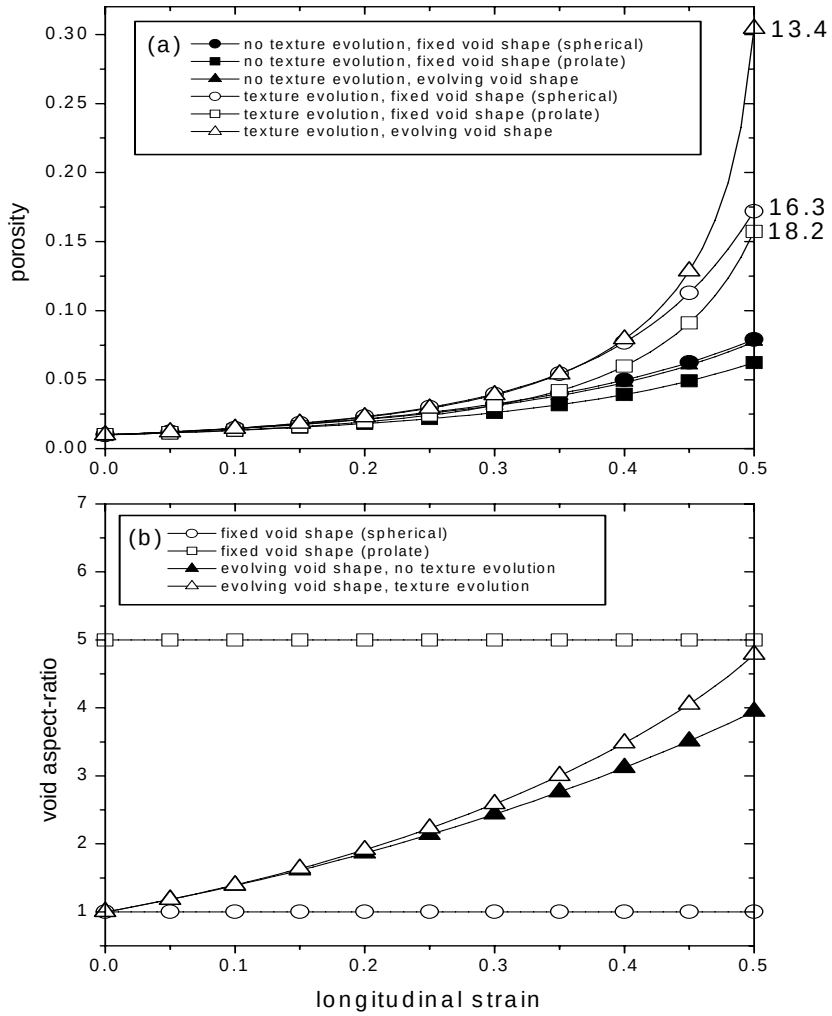

Figure 8. Effect of texture development. Evolution of (a) porosity and (b) void aspect ratio during a creep test performed on an fcc polycrystal with random texture for different void morphologies with and without texture or morphology evolution. Initial porosity 1%, X = 1, n = 10, total longitudinal strain 0.5. In the cases with texture evolution, the final (111) inverse pole figure maximum is indicated in the right margin.

crystallographic texture development is allowed, in all the cases the final porosities remain below 10%. As discussed in Section 3.4, prolate voids tend to grow slower than spherical voids. Moreover, if the initially spherical voids are allowed to evolve in shape under such a stress state, they become prolate and the porosity exhibits a slightly slower evolution. On the other hand, if the crystallographic texture is allowed to evolve, two things happen: the tensile axis tends to align with the <111> crystallographic direction (a secondary component develops along the <100> direction) and the solid phase (grains) become harder to deform along this direction. As a consequence, more deformation is accommodated by the void phase (compare open and solid symbol curves). In the cases of fixed void shape, once again, prolate voids grow slower than

spherical voids. In the case of evolving shape, although the voids go from spherical to prolate shape, the porosity grows even faster than in the former cases, indicating a strong coupling between texture, morphologic effects, and porosity evolution. Illustrating the effect of porosity on texture in Fig. 8a, we report the final intensities of the <111>-peak of the inverse pole figure, corresponding to the three cases with texture evolution. It can be seen that if the porosity evolves faster (slower), the deformation carried out by the solid material is smaller (higher), leading to a slower (faster) crystallographic texture evolution. Finally, Fig. 8b shows that the evolving morphology of the cavities is also affected by the anisotropy evolution of the voided polycrystal. Comparing the void aspect ratio predicted with and without crystallographic texture evolution, it is seen that in the former case the voids become more elongated than in the latter case for the same amount of macroscopic elongation.

The previous example shows that the anisotropy induced by texture development in a polycrystal with initial random texture gradually affects the porosity evolution. As a consequence, it is to be expected that a simulation carried out in an initially textured polycrystal along different directions should predict a different trend of void growth from the very beginning of the deformation. Furthermore, this anisotropic behavior should be more marked if the plastic anisotropy of the single crystal is higher. For this reason, the next example concerns an hcp material with easy $(0001)<1\bar{2}10>$ basal and $(10\bar{1}0)<1\bar{2}10>$ prismatic <a> slip and four times harder $(10\bar{1}1)<11\bar{2}3>$ pyramidal <c+a> slip. The initial texture consists of a strong basal component along the axis x_1 (see Fig. 9b). Imposing axisymmetric tensile states parallel to the axis x_1 or perpendicular to it (along axis x_2) for triaxialities X = 1/3 and X = 1, for an initial concentration $\phi = 0.01$ of spherical voids and for a final longitudinal strain of 0.5, we observe that (1) texture evolution is not very sensitive to triaxiality and rather depends on the relative orientation of the initial texture and the tensile axis (Fig. 9b), and (2) the porosity evolution is strongly influenced by the texture, especially at higher triaxialities (Fig. 9a). Indeed, the case of tension along x_1 (i.e., most crystals with their <c>-axis aligned in tensile direction and therefore hard to deform) exhibits a faster void growth than the case of tension along x_2, and the reason is clear: the material chooses to accommodate deformation by opening the voids rather than by deforming plastically along the hard direction. The coupling between the hydrostatic component and the material plastic anisotropy is strong: for triaxiality X = 1, the hydrostatic component

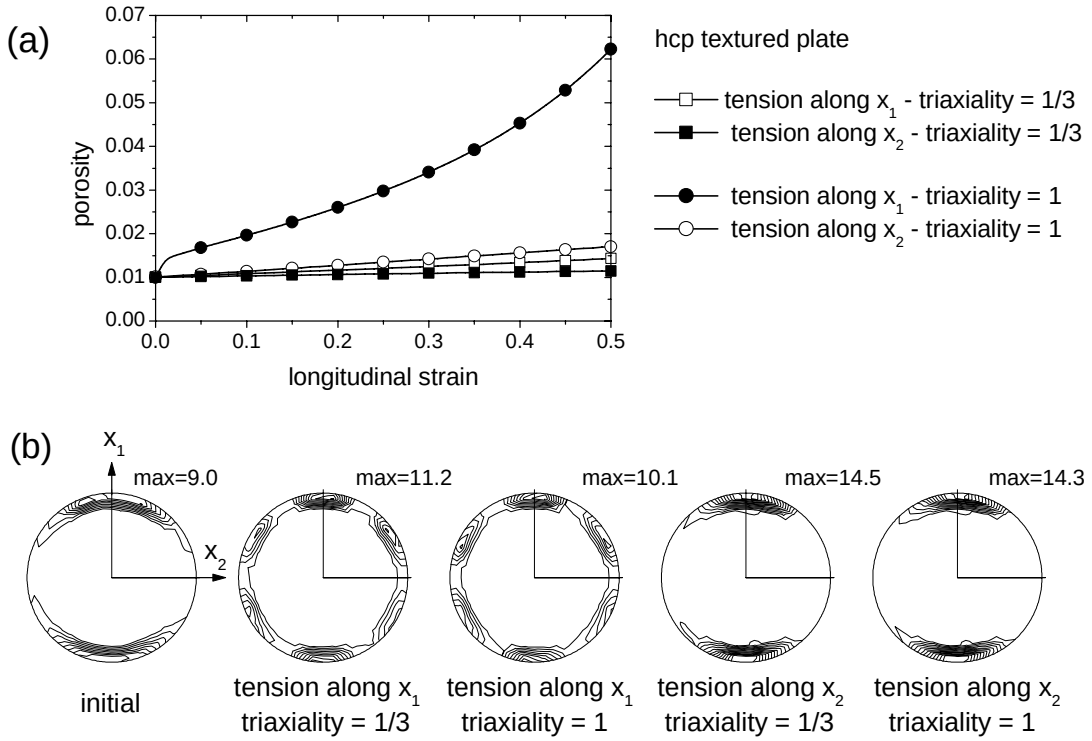

Figure 9. Coupling between initial texture and porosity evolution. VPSC predictions of (a) porosity evolution in an initially textured hcp polycrystal deformed in tension along x_1 and x_2 for triaxialities 1/3 and 1. Initial porosity 1%, n = 10; prismatic and basal slip (τ^s = 100 MPa) and pyramidal <c+a> slip (τ^s = 400 MPa) modes; total longitudinal strain 0.5. (b) Initial and final (0001) basal poles figures for the four cases shown above.

leverages the latter mechanism and promotes an acceleration in void contribution to deformation (Fig. 9a). The response of the hcp aggregate provides a dramatic example of a case where the combined anisotropy of the single crystal and of the polycrystal (texture) affect the evolution of porosity substantially.

The difference in porosity evolution predicted above when the textured hcp plate is made to creep in tension along different directions should also manifest itself in the overall mechanical response. Figure 10 shows the predicted stress-strain curves obtained by imposing a constant axial strain rate of 1 s^{-1} and a constant lateral stress chosen to give an initial triaxiality of 1. Note that unlike a creep test simulation, these mixed-boundary conditions determine changes in triaxiality (in these cases, an increase) as deformation proceeds. Other parameters of these simulations were n = 10, 1% initial porosity, texture and morphology evolution allowed, and no mechanical strain-hardening (i.e., constant threshold stresses for every slip system throughout

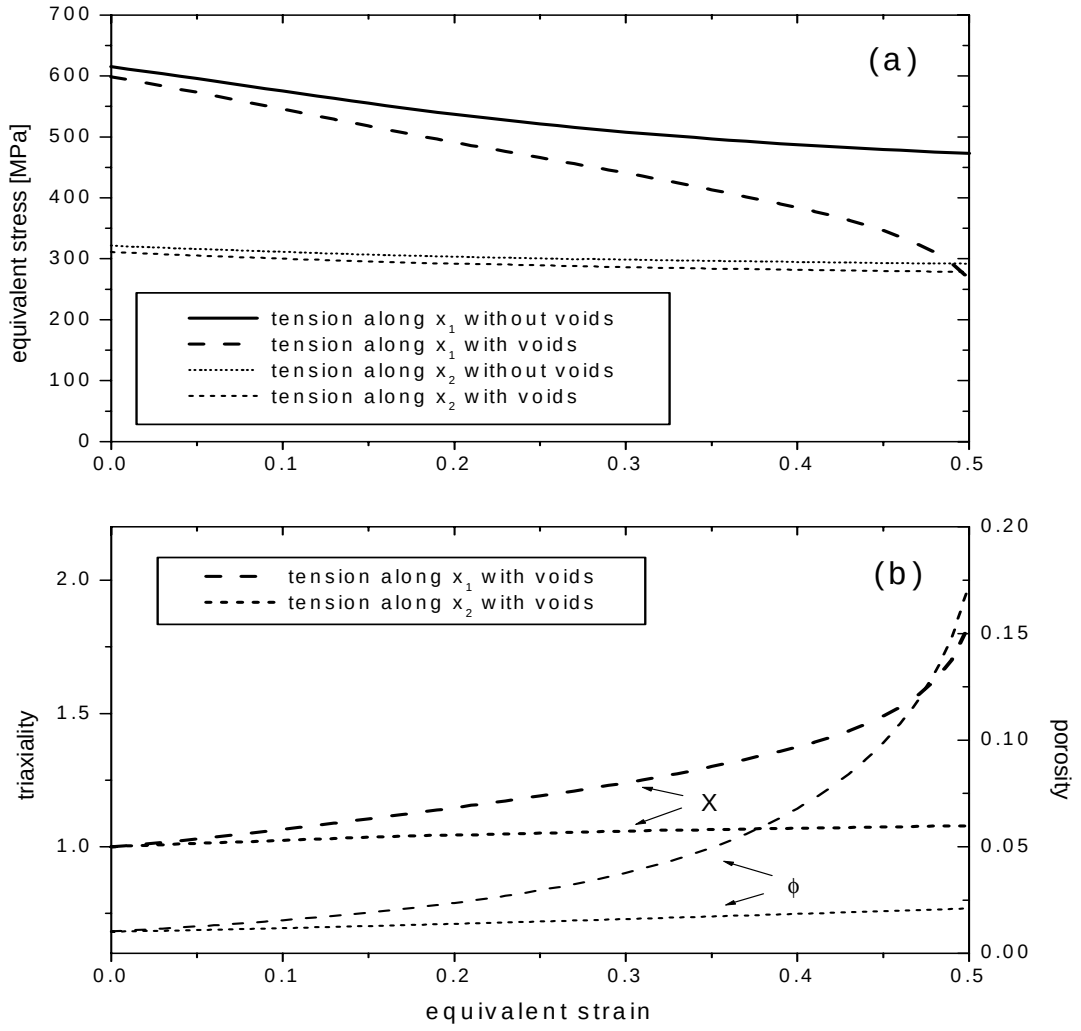

Figure 10. Influence of porosity evolution on macroscopic mechanical behavior. (a) Stress-strain curves calculated with VPSC for the textured hcp polycrystal of Fig. 9b deformed in tension along both in-plane directions at a constant longitudinal strain rate of 1 s^{-1} and imposing constant lateral stresses to give an initial triaxiality of 1. Cases with and without porosity. (b) Porosity (right axis) and triaxiality (left axis) evolution. Initial porosity 1%, n = 10, total longitudinal strain 0.5.

deformation). In order to assess the influence of porosity evolution, Fig. 10 also shows the stress-strain curves without porosity, which shows a geometric softening consistent with the texture evolution shown in Fig. 9b. In the case of tension along x_1, a fast porosity evolution induces a significant additional softening (and, consequently, a marked increase of the triaxiality), while in the case of tension along x_2, the contribution to softening of the slow porosity evolution is only marginal.

4. CONCLUSIONS

We have presented here an extension of the polycrystal VPSC model that incorporates a viscoplastic compressibility into the originally incompressible approach. The motivation for this extension is to be able to account for dilatational damage and its evolution during plastic-forming while retaining the capabilities of the original VPSC formulation. Specifically, we are interested in retaining the crystallographic basis of the model and its description of anisotropy and anisotropy evolution both at the grain and at the aggregate level. We also retain the rate sensitivity effects built into the model. The benefits of extending the VPSC formulation, however, go beyond the specific problem of damage evolution. By forcing us to reformulate the model in terms of a more general linearization of the material response (which supersedes the traditional secant or tangent assumptions), we can now account (albeit approximately) for variations of stress and strain rates in the grains. Such a super-tangent extension is based on the affine formulation for viscoplasticity proposed by Masson et al. (2000).

It is unavoidable when referring to plasticity models that include porosity to compare them with the widely used seminal model proposed by Gurson (1977). The present VPSC extension has advantages and disadvantages when compared to the Gurson model. Among the advantages:

1) VPSC accounts for the anisotropy of the mechanical response, while Gurson is limited to an isotropic response;
2) VPSC accounts for ellipsoidal void shapes and shape evolution with deformation, while Gurson assumes spherical voids; and
3) Rate-sensitivity effects are not accounted for by the Gurson formulation.

Among the disadvantages:

1) VPSC is based on a linearization of a highly nonlinear rate-sensitive constitutive response and, as a consequence, it becomes less accurate when spatial inhomogeneity is large. This handicap is partially mitigated with the introduction of the super-tangent approach;
2) VPSC cannot handle purely hydrostatic stress states, although from an algorithmic point of view it can handle stress triaxilities up to X = 20; and

3) From a numerical point of view, VPSC is much more complex to implement than Gurson and much more demanding on computer resources. In addition, the fact that the VPSC formulation starts deviating from the accepted associative rule at triaxialities of order X = 5 may represent an advantage over the Gurson formulation, which assumes the validity of the latter rule.

Obviously, the reason for choosing VPSC over Gurson (or over one of the various Gurson extensions proposed in the literature) depends on the characteristics of the material and the loading conditions under consideration. When anisotropy and its evolution with deformation has to be accounted for, or when void shape matters, then we show in this work that VPSC performs well when simulating the mechanical response and porosity evolution. We may say that, in much the same way as the original VPSC formulation represents an improvement over the limited isotropic Von Mises plastic approach, the present extension represents an improvement over the simple isotropic Gurson formulation.

The extended VPSC model contains one tunable parameter, $\alpha(\phi, X)$, a function of the porosity and the triaxilality that controls the linearization of the constituive response. This function is tuned to give the same response as Gurson when the material has low rate sensitivity, is isotropic, and the cavities are spherical. A direct connection exists between this parameter and the second-order stress moment associated with the stress gradients in the grains, which are required to accommodate locally the deformation of the voids. Such second-order moment dependence was formally introduced by Ponte Castañeda (1991, 2002a,b) in his variational formalisms.

We explore here the predictions of the extended VPSC formulation for a variety of situations. Specifically, we test the effect of void shape, texture, strain rate, and triaxiality upon damage evolution, texture evolution, and stress-strain response. In all these cases, the results obtained are qualitatively in agreement with the intuitive response that one expects. For example, we predict that

1) Void shape has a major effect on porosity evolution. Oblate voids tend to grow faster than prolate voids under tensile stress, and lead to accelerated damage evolution.

2) Rate-sensitivity influences porosity evolution in such a way that, under tensile stress, voids tends to grow faster in less rate-sensitive materials.

3) Porosity evolution does not substantially affect texture evolution in comparison with an aggregate without voids that is deformed to the same strain.

4) Texture can change substantially the porosity evolution in a highly anisotropic hexagonal aggregate tested along and across the basal component. The reason is that it is more efficient for the material to accommodate deformation by deforming the voids rather than by deforming the hard direction of the grains.

5) Superimposing a hydrostatic stress component increases the rate of void dilatation and, consequently, their contribution to deformation.

This extended VPSC model will have to be tested and expanded in the future. Experimental verification should be an important part of such efforts, and producing materials with controlled initial porosity and texture and performing well-controlled experiments will certainly be a challenge. From a numerical perspective, we plan to use the model to describe the local constitutive response in FEM simulations of plastic-forming operations. Criteria for void nucleation can be incorporated into the formulation in a straightforward manner, as well as distributions of void shapes. It will be more challenging to incorporate void coalescence effects and a dependence of the model with the relative size of voids and grains (size effects). Finally, we plan to study the model's performance when simulating aggregates of material grains (no voids) with very inhomogeneous properties. The possibility of accounting for intragranular gradients and localization through second-order moments should open new avenues in this area and should provide a more efficient tool for looking into these systems.

ACKNOWLEDGMENTS

The authors wish to thank Prof. Pedro Ponte Castañeda for fruitful discussions.

REFERENCES

Addessio, F.L., and J.N. Johnson, "Rate-dependent ductile fracture model," *J. Appl. Phys.* **74**, 1640–1648 (1993).

Berveiller, M., O. Fassi-Fehri, and A. Hihi, "The problem of two plastic and heterogeneous inclusions in an anisotropic medium," *Int. J. Eng. Sci.* **25**, 691–709 (1987).

Carroll, M.M., and A.C. Holt, "Static and dynamic pore-collapse relations for ductile porous materials," *J. Appl. Phys.* **43**, 1626–1636 (1972).

Chen, B., Y. Huang, C. Liu, P.D. Wu, and S.R. MacEwen, "A dilatational plasticity theory for viscoplastic materials" (submitted to *Eng. Fract. Mech.*).

Chen, B., Z.C. Xia, S.R. MacEwen, S.C. Tang, and Y. Huang, "A dilatational plasticity theory for aluminum sheets," in *Multiscale deformation and fracture in materials and structures,* T.J. Chuang and J.W. Rudnicki, Eds. (Kluwer Academic Publishers, Dordrecht, Netherlands, 2000), pp. 17–30.

Golaganu, M., J.B. Leblond, and J. Devaux, "Approximate models for ductile metals containing non-spherical voids–case of axisymmetric prolate ellipsoidal cavities," *J. Mech. Phys. Solids* **41**, 1723–1754 (1993).

Golaganu, M., J.B. Leblond, and J. Devaux, "Approximate models for ductile metals containing non-spherical voids–case of axisymmetric oblate ellipsoidal cavities," *J. Eng. Mater. Technol.* **116**, 290–287 (1994).

Gurson, A.L., "Continuum theory of ductile rupture by void nucleation and growth," *J. Eng. Mater. Technol.* **99**, 2–15 (1977).

Hutchinson, J.W., "Bounds and self-consistent estimates for creep of polycrystalline materials," *Proc. R. Soc. London, Ser. A* **348**, 101–27 (1976).

Johnson, J.N., and F.L. Addessio, "Tensile plasticity and ductile fracture," *J. Appl. Phys.* **64**, 6699–6712 (1988).

Kailasam, M., P. Ponte Castañeda, and J.R. Willis, "The effect of particle size, shape, distribution and their evolution on the constitutive response of nonlinearly viscous composites. I–Theory," *Proc. R. Soc. London, Ser. A* **355**, 1835–1852 (1997a).

Kailasam, M., P. Ponte Castañeda, and J.R. Willis, "The effect of particle size, shape, distribution and their evolution on the constitutive response of nonlinearly viscous composites. II–Examples," *Proc. R. Soc. London, Ser. A* **355**, 1853–1872 (1997b).

Kailasam, M., N. Aravas, and P. Ponte Castañeda, “Porous metals with developing anisotropy: constitutive models, computational issues and applications to deformation processing,” *CMES* 1, 105–118 (2000).

Lebensohn, R.A., and G.R. Canova, “A self-consistent approach for modeling texture development of two-phase polycrystals: Application to titanium alloys,” *Acta Metall. Mater.* **45**, 3687–3694 (1997).

Lebensohn, R., D. Solas, G. Canova, and Y. Brechet, “Modeling damage of Al-Zn-Mg alloys,” *Acta Metall. Mater.* **44**, 315–325 (1996).

Lebensohn, R.A., and C.N. Tomé, “A self-consistent approach for the simulation of plastic deformation and texture development of polycrystals: Application to zirconium alloys,” *Acta Metall. Mater.* **41**, 2611 (1993).

Lebensohn, R.A, P.A. Turner, J.W. Signorelli, G.R. Canova, and C.N. Tomé, “Calculation of intergranular stresses based on a large strain viscoplastic self-consistent polycrystal model,” *Mod. Sim. Mat. Sci. Eng*. **6**, 447–465 (1998).

Lee, B.J., and M.E. Mear, “Axisymmetric deformation of power-law solids containing a dilute concentration of aligned spheroidal voids,” *J. Mech. Phys. Solids* **39**, 45–71 (1991).

Liu, C., Y. Huang, and M.G. Stout, “On the application of Gurson’s theory to voided solids with rate sensitive matrices” [In preparation. 2002].

Logé, R., Y. Chastel, J. Signorelli, R. Lebensohn, P. Barberis, “Finite element simulation of a zircaloy sheet deep drawing using a polycrystalline model,” in *Simulation of materials processing: Theory, methods and applications*, J. Huétink and F.P.T. Baaijens, Eds. (Balkema, Rotterdam, Netherlands, 1998), pp. 329–333.

Masson, R., M. Bornert, P. Suquet, and A. Zaoui, “An affine formulation for the prediction of the effective properties of nonlinear composites and polycrystals,” *J. Mech. Phys. Solids* **48**, 1203–1227 (2000).

Molinari, A., G.R. Canova, and S. Ahzi, “A self-consistent approach of the large deformation polycrystal viscoplasticity,” *Acta Metall. Mater.* **35**, 2983–2994 (1987).

Mura, T., *Micromechanics of Defects in Solids* (Martinus-Nijhoff, Dordrecht, Netherlands, 1988).

Ponte Castañeda, P., "The effective mechanical properties of nonlinear isotropic composites," *J. Mech. Phys. Solids* **39**, 45–71 (1991).

Ponte Castañeda, P., "Exact second-order estimates for the effective mechanical properties of non-linear composite materials," *J. Mech. Phys. Solids* **44**, 827–862 (1996).

Ponte Castañeda, P., "Second-order homogeneization estimates for nonlinear composites incorporating field fluctuations. I—Theory," *J. Mech. Phys. Solids* **50**, 737–757 (2002a).

Ponte Castañeda, P., "Second-order homogeneization estimates for nonlinear composites incorporating field fluctuations. I—Applications," *J. Mech. Phys. Solids* **50**, 759–782 (2002b).

Ponte Castañeda, P., and M. Zaidman, "Constitutive models for porous materials with evolving microstructure," *J. Mech. Phys. Solids* **42**, 1459–1497 (1996).

Suquet, P., "Overall properties of non-linear composites: A modified secant moduli theory and its link with Ponte Castañeda's nonlinear variational procedure," *C.R. Acad Sci. Paris IIb* **320**, 563–571 (1995).

Taylor, G.I., "Plastic strain in metals," *J. Inst. Metals* **62**, 307–324 (1938).

Tomé, C.N., P.J. Maudlin, R.A. Lebensohn, and G.A. Kaschner, "Mechanical response of zirconium. Part I—Derivation of a polycrystal constitutive law and finite element analysis," *Acta Metall. Mater*. **49**, 3085–3096 (2001).

Tveergard, V., "Influence of voids on shear bands instabilities under plane strain conditions," *Int. J. Fracture* **17**, 389–407 (1981).

Tveergard, V., "On localization in ductile materials containing spherical voids," *Int. J. Fracture* **18**, 237–252 (1982).

Walpole, L.J., "On the overall elastic moduli of composite materials," *J. Mech. Phys. Solids* **17**, 235–251 (1969).

APPENDIX A. INTEGRATION OF $\Lambda(\bar{\alpha})$ OVER ELLIPSOIDAL DOMAINS

The use of the Fourier transform for solving the differential system (7) plus the integration of the velocity gradient field inside the domain of a grain to get average representative values of the velocity gradient in the grain leads to integrals of the form (37),

$$\Lambda(\bar{\alpha}) = \int_0^{\infty} \left(\int_{\Omega}\int_{\Omega} \exp\left[-i\bar{k}(\bar{x}-\bar{x}')\right] d\bar{x}\, d\bar{x}' \right) k^2 dk \ , \tag{A1}$$

which can be rewritten as

$$\Lambda(\bar{\alpha}) = \int_0^{\infty} \left(\int_{\Omega} \exp\left(-i\bar{k}\bar{x}\right) d\bar{x} \int_{\Omega} \exp\left(i\bar{k}\bar{x}'\right) d\bar{x}' \right) k^2 dk \ . \tag{A2}$$

Solving the integrals in the Cartesian space over the ellipsoidal domain of radii (a,b,c) gives

$$\int_{\Omega} \exp\left(-i\bar{k}\bar{x}\right) d\bar{x} \ = 4\pi abc \frac{\sin\left[\rho(\bar{\alpha})k\right] - \left[\rho(\bar{\alpha})k\right]\cos\left[\rho(\bar{\alpha})k\right]}{\left[\rho(\bar{\alpha})k\right]^3} \ , \tag{A3}$$

where $\rho(\bar{\alpha}) = \sqrt{(a\alpha_1)^2 + (b\alpha_2)^2 + (c\alpha_3)^2}$ and $\bar{k} = k\bar{\alpha}$. Since the right term in (A3) is an even function of k, the same result holds for $\int_{\Omega} \exp\left(i\bar{k}\bar{x}\right) d\bar{x}$. Replacing (A3) in (A2), we obtain

$$\Lambda(\bar{\alpha}) = \frac{(4\pi abc)^2}{\left[\rho(\bar{\alpha})\right]^6} \int_0^{\infty} \frac{\left(\sin\left[\rho(\bar{\alpha})k\right] - \left[\rho(\bar{\alpha})k\right]\cos\left[\rho(\bar{\alpha})k\right]\right)^2}{k^4} dk \ . \tag{A4}$$

Solving the improper integral in (A4) gives (Bervellier et al., 1987)

$$\int_0^{\infty} \frac{\left(\sin\left[\rho(\bar{\alpha})k\right] - \left[\rho(\bar{\alpha})k\right]\cos\left[\rho(\bar{\alpha})k\right]\right)^2}{k^4} dk = \frac{\pi}{6}\left[\rho(\bar{\alpha})\right]^3$$

Hence,

$$\Lambda(\bar{\alpha}) = \frac{8\pi^3}{3} \frac{(abc)^2}{\left[\rho(\bar{\alpha})\right]^3} \ . \tag{A5}$$

APPENDIX B. CALCULATION OF THE LOCAL MEAN STRESS FIELD

The local deviation of the mean stress represents the fourth unknown in the system (7) of differential equations. Using the solution for the associated Green tensor $H_m(\bar{x})$, the local deviation of the mean stress can be expressed as the convolution integral

$$\begin{aligned} \tilde{\sigma}^s(\bar{\mathbf{x}}) &= \int_{R^3} H_m(\bar{\mathbf{x}}-\bar{\mathbf{x}}')\, f_m(\bar{\mathbf{x}}')\, d\bar{x}' \qquad (m=1,4)\,, \\ \tilde{\sigma}^s(\bar{\mathbf{x}}) &= \int_{R^3} H_i(\bar{\mathbf{x}}-\bar{\mathbf{x}}')\, f_i^d(\bar{\mathbf{x}}')\, d\bar{x}' + \int_{R^3} H_4(\bar{\mathbf{x}}-\bar{\mathbf{x}}')\, f^s(\bar{\mathbf{x}}')\, d\bar{x}' \qquad (i=1,3)\,, \end{aligned} \tag{B1}$$

where the fictitious forces are defined by Eqs. (8) and (9). Following the procedure described in Section 2.3, we assume uniform eigenstrain rate within the domain Ω of the grain and zero outside and calculate the average mean stress deviation within the grain's volume. Integrating (B1) gives

$$\tilde{\sigma}^s = -\frac{1}{\Omega}\int_\Omega\int_\Omega H_i(\bar{x}-\bar{x}')\,\bar{L}_{ijkl}\dot{\varepsilon}^{d*}_{kl,j}(\bar{x}')\,d\bar{x}d\bar{x}' - \frac{1}{\Omega}\int_\Omega\int_\Omega H_4(\bar{x}-\bar{x}')\,\bar{K}\dot{\varepsilon}^{s*}(\bar{x}')d\bar{x}d\bar{x}'. \tag{B2}$$

Solving the first integral by parts and using the divergence theorem, we obtain

$$\tilde{\sigma}^s = -\frac{1}{\Omega}\int_\Omega\int_\Omega H_{i,j}(\bar{x}-\bar{x}')\,\bar{L}_{ijkl}\dot{\varepsilon}^{d*}_{kl}\,d\bar{x}d\bar{x}' - \frac{1}{\Omega}\int_\Omega\int_\Omega H_4(\bar{x}-\bar{x}')\,\bar{K}\dot{\varepsilon}^{s*}\,d\bar{x}d\bar{x}'. \tag{B3}$$

Next, using the definition of the Fourier transform, Eq. (19b),

$$\begin{aligned} \tilde{\sigma}^s = {} & \frac{-1}{8\pi^3\Omega}\left(\int_\Omega\int_\Omega\int_{R^3}\hat{H}_i(\bar{k})(-ik_j)\exp[-i\bar{k}(\bar{x}-\bar{x}')]\,d\bar{k}d\bar{x}d\bar{x}'\right)\bar{L}_{ijkl}\dot{\varepsilon}^{d*}_{kl} - \\ & \frac{1}{8\pi^3\Omega}\left(\int_\Omega\int_\Omega\int_{R^3}\hat{H}_4(\bar{k})\exp[-i\bar{k}(\bar{x}-\bar{x}')]\;d\bar{k}d\bar{x}d\bar{x}'\right)\bar{K}\dot{\varepsilon}^{s*}\,. \end{aligned} \tag{B4}$$

Using the explicit form of the inverse Fourier transform, Eqs. (27) and (28),

$$\begin{aligned} \tilde{\sigma}^s = {} & \frac{1}{8\pi^3\Omega}\left(\int_\Omega\int_\Omega\int_{R^3}A^{-1}_{4i}(\bar{\alpha})\alpha_j\exp[-i\bar{k}(\bar{x}-\bar{x}')]\,d\bar{k}d\bar{x}d\bar{x}'\right)\bar{L}_{ijkl}\dot{\varepsilon}^{d*}_{kl} + \\ & \frac{1}{8\pi^3\Omega}\left(\int_\Omega\int_\Omega\int_{R^3}A^{-1}_{44}(\bar{\alpha})\exp[-i\bar{k}(\bar{x}-\bar{x}')]\;d\bar{k}d\bar{x}d\bar{x}'\right)\dot{\varepsilon}^{s*}\,. \end{aligned} \tag{B5}$$

Writing $d\bar{k}$ in spherical coordinates $d\bar{k} = k^2 \sin\theta \, dk \, d\theta \, d\varphi$ and using the integral derived in Appendix A reduces (B5) to

$$\tilde{\sigma}^s = \left(\frac{abc}{4\pi} \int_0^{2\pi} \int_0^{\pi} \frac{A_{4i}^{-1}(\bar{\alpha})\alpha_j}{[\rho(\bar{\alpha})]^3} \sin\theta d\theta d\varphi \right) \bar{L}_{ijkl} \, \dot{\varepsilon}_{kl}^{d*} + \left(\frac{abc}{4\pi} \int_0^{2\pi} \int_0^{\pi} \frac{A_{44}^{-1}(\bar{\alpha})}{[\rho(\bar{\alpha})]^3} \sin\theta d\theta d\varphi \right) \dot{\varepsilon}^{s*} , \qquad \text{(B6)}$$

where $\rho(\bar{\alpha}) = \left[(a\alpha_1)^2 + (b\alpha_2)^2 + (c\alpha_3)^2 \right]^{1/2}$, and the first bracket is the tensor T_{ij}^s obtained in Section 2.3 (Eq. 41), in connection with the velocity gradient deviations. As a matter of fact, a reduced form of the expression (B6) containing only the first term was derived by Lebensohn et al. (1998) for the solution of the incompressible inclusion in an incompressible medium. The first term in (B6) couples the deviations in mean stress to the deviatoric eigenrate, while the second term arises from the compressibility of the medium and couples the deviation in mean stress with the dilatational eigenrate.

APPENDIX C. COMPARISON BETWEEN THE NORMS OF ξ_{ijmn} AND S^{d}_{ijmn}

In Section 2.3, the tensor $\xi_{ijmn} = \dfrac{S^{s}_{ij} S^{d}_{kkmn}}{\Psi}$ present in Eq. (48) that relates the deviatoric strain-rate deviation and the deviatoric eigenstrain rate

$$\tilde{\dot{\varepsilon}}^{d}_{ij} = \left(S^{d}_{ijmn} - \xi_{ijmn}\right)\dot{\varepsilon}^{d*}_{mn} + \beta_{ij}\tilde{\dot{\varepsilon}}^{s} \tag{C1}$$

was removed from the above equation to give

$$\tilde{\dot{\varepsilon}}^{d}_{ij} \cong S^{d}_{ijmn}\ \dot{\varepsilon}^{d*}_{mn} + \beta_{ij}\tilde{\dot{\varepsilon}}^{s} \tag{C2}$$

by arguing that, in general, $\left\|\xi_{ijmn}\right\| << \left\|S^{d}_{ijmn}\right\|$. The following numerical examples illustrate the latter inequality. Figure C1 shows the cases of two different creep test simulations (no texture or morphology evolution allowed) of fcc polycrystals with random texture, for different triaxialities and void shapes. Figure C1a shows the quadratic norms of ξ_{ijmn} and S^{d}_{ijmn} and the porosity evolution for X = 1, spherical voids, 1% initial porosity, 0.5 final longitudinal strain, and around 10% final porosity. In this case, $\left\|\xi_{ijmn}\right\|_2$ remains several orders of magnitudes smaller than $\left\|S^{d}_{ijmn}\right\|_2$ throughout the simulation. Figure C1b shows the results of another creep test simulation for a higher triaxiality (X = 3) and a faster porosity evolution, induced by the oblate morphology of the voids (aspect ratio 1:1:5) with an initial porosity of 3×10^{-4}, a final longitudinal strain of 0.09, and around 10% final porosity. In this case, $\left\|\xi_{ijmn}\right\|_2$ shows a rapid increase as porosity increases but it still remains two orders of magnitude below $\left\|S^{d}_{ijmn}\right\|_2$ at the end the simulation.

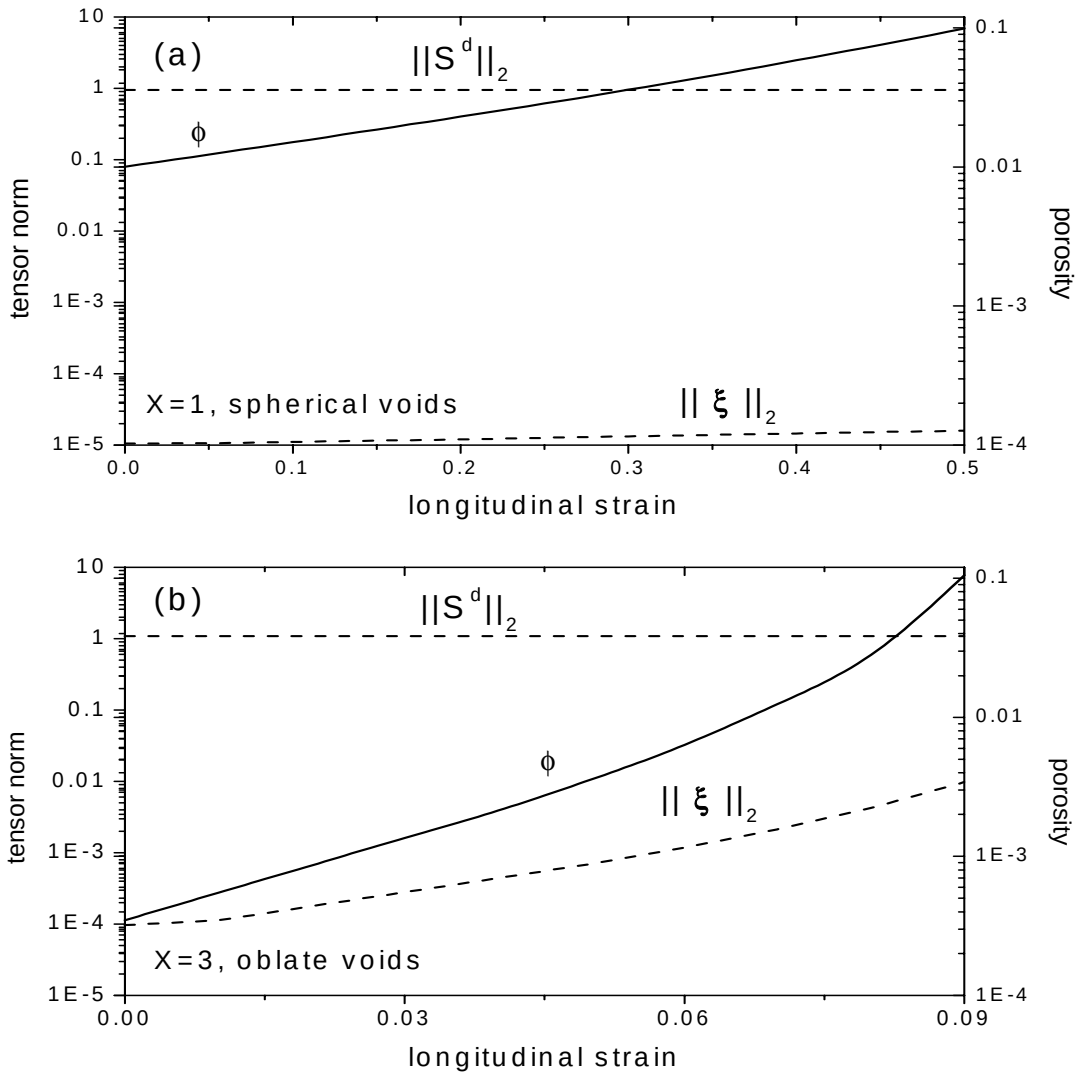

Figure C1. Comparison between the norms of the tensors ξ_{ijmn} and S^d_{ijmn} (dashed lines, right axis scale) in creep test simulations on random fcc polycrystals. Cases: (a) 1% initial porosity, X = 1, spherical voids, n = 10, final longitudinal strain 0.5. (b) Initial porosity 3×10^{-4}, X = 3, oblate voids (1:1:5), final longitudinal strain 0.09. No texture or morphology evolution allowed. The porosity evolution is superimposed (solid line, right axis scale).

APPENDIX D. SELF-CONSISTENT EQUATIONS FOR AGGREGATES WITH DIFFERENT GRAIN AND VOID SHAPES

In Section 2.4, we derived the following interaction equations (Eq. 56):

$$\dot{\varepsilon}_{ij}^{d} - \dot{E}_{ij}^{d} = -\tilde{M}_{ijkl}\left(\sigma_{kl}^{d} - \Sigma_{kl}^{d}\right) - \tilde{\beta}_{kl}\tilde{\sigma}^{s} \,, \tag{D1a}$$

$$\dot{\varepsilon}^{s} - \dot{E}^{s} = -\tilde{K}^{-1}\left(\sigma^{s} - \Sigma^{s}\right) . \tag{D1b}$$

The unknown moduli of the effective medium follow from enforcing the condition that the volumetric average of stress and strain rates has to coincide with the macroscopic magnitudes

$$\Sigma_{kl}^{d} = \left\langle \sigma_{kl}^{d} \right\rangle, \quad \Sigma^{s} = \left\langle \sigma^{s} \right\rangle, \tag{D2}$$

$$\dot{E}_{kl}^{d} = \left\langle \dot{\varepsilon}_{kl}^{d} \right\rangle, \quad \dot{E}^{s} = \left\langle \dot{\varepsilon}^{s} \right\rangle. \tag{D3}$$

If the shape and orientation of the ellipsoids that represent the grains and the voids are the same, then the Eshelby tensors S_{ijkl}^{d}, S_{ij}^{s}, and the Eshelby factor Ψ are the same for all grains and voids and, as a consequence, the interaction tensors and factors $\tilde{M}_{ijkl}$ and $\tilde{K}$ are the same for every grain and void in the aggregate. Hence, when taking the average in (D1), these magnitudes can be factored out from the average to give

$$\left\langle \dot{\varepsilon}_{ij}^{d} \right\rangle - \dot{E}_{ij}^{d} = -\tilde{M}_{ijkl}\left(\left\langle \sigma_{kl}^{d} \right\rangle - \Sigma_{kl}^{d}\right), \tag{D4a}$$

$$\left\langle \dot{\varepsilon}^{s} \right\rangle - \dot{E}^{s} = -\tilde{K}^{-1}\left(\left\langle \sigma^{m} \right\rangle - \Sigma^{m}\right). \tag{D4b}$$

Note that in writing (D4), we used $\left\langle \tilde{\beta}_{kl}\tilde{\sigma}^{s} \right\rangle = \tilde{\beta}_{kl}\left\langle \tilde{\sigma}^{s} \right\rangle = 0$. From Eq. (D4) it is obvious that if the conditions (D2) on the stress components are fulfilled, then the conditions (D3) on the strain-rate components follow automatically and vice versa. However, if the grain and void shapes differ, then their Eshelby tensors are also different, and consequently, $\tilde{M}_{ijkl}$ and $\tilde{K}$ cannot be factored out from the averages. In this case, a more general formulation is required in order to fulfill simultaneously the stress and strain-rate averages (Walpole, 1969; Lebensohn et al., 1996). First, let us define the auxiliary magnitudes $\Sigma_{ij}^{d\bullet}$, $\Sigma^{s\bullet}$, $\dot{E}_{ij}^{d\bullet}$, and $\dot{E}^{s\bullet}$, related through the macroscopic constitutive law Eq. (3),

$$\dot{E}_{ij}^{d\bullet} = \overline{M}_{ijkl}\,\Sigma_{kl}^{d\bullet} + \dot{E}_{ij}^{do}\ , \tag{D5a}$$

$$\dot{E}^{s\bullet} = \overline{K}^{-1}\,\Sigma^{s\bullet}\ . \tag{D5b}$$

Subtracting equations (D5) from equations (53) and following the procedure leading to the interaction equation (D1) gives another form of the interaction equations,

$$\dot{\varepsilon}_{ij}^{d} - \dot{E}_{ij}^{d\bullet} = -\widetilde{M}_{ijkl}\left(\sigma_{kl}^{d} - \Sigma_{kl}^{d\bullet}\right) - \widetilde{\beta}_{kl}\tilde{\sigma}^{s}\ , \tag{D6a}$$

$$\dot{\varepsilon}^{s} - \dot{E}^{s\bullet} = -\widetilde{K}^{-1}\left(\sigma^{s} - \Sigma^{s\bullet}\right). \tag{D6b}$$

Now we need to determine the auxiliary magnitudes using the conditions (D2) and (D3). From (D6a) we obtain the following localization relation:

$$\sigma_{ij}^{d} = B_{ijkl}\,\Sigma_{ij}^{d\bullet} + \Phi_{ij}\ , \tag{D7}$$

where B_{ijkl} and Φ_{ij} are given by Eq. (59). Taking average in Eq. (D7),

$$\Sigma_{ij}^{d} = \left\langle \sigma_{ij}^{d} \right\rangle = \left\langle B_{ijkl} \right\rangle \Sigma_{kl}^{d\bullet} + \left\langle \Phi_{ij} \right\rangle\ . \tag{D8}$$

Hence,

$$\Sigma_{ij}^{d\bullet} = \left\langle B_{ijkl} \right\rangle^{-1}\left(\Sigma_{kl}^{d\bullet} - \left\langle \Phi_{kl} \right\rangle\right). \tag{D9}$$

Then, replacing (D9) in (D7) to remove the auxiliary stress $\Sigma_{ij}^{d\bullet}$,

$$\sigma_{ij}^{d} = B_{ijkl}\left[\left\langle B_{klmn} \right\rangle^{-1}\left(\Sigma_{mn}^{d} - \left\langle \Phi_{mn} \right\rangle\right)\right] + \Phi_{ij}\ . \tag{D10}$$

Using the local constitutive law (53a), and following the same procedure as in Section 2.4, we obtain

$$\dot{\varepsilon}_{ij}^{d} = M_{ijkl}\,B_{klmn}\left(\left\langle B_{klmn} \right\rangle^{-1}\left(\Sigma_{mn}^{d} - \left\langle \Phi_{mn} \right\rangle\right)\right) + M_{ijkl}\,\Phi_{kl} + \dot{\varepsilon}_{ij}^{do}\ , \tag{D11}$$

$$\begin{aligned} \overline{M}_{ijpq}\,\Sigma_{pq}^{d} + \dot{E}_{ij}^{do} = \dot{E}_{ij}^{d} = \left\langle \dot{\varepsilon}_{ij}^{d} \right\rangle = \left\langle M_{ijkl}\,B_{klmn} \right\rangle \left\langle B_{mnpq} \right\rangle^{-1} \Sigma_{pq}^{d} \\ - \left\langle M_{ijkl}\,B_{klmn} \right\rangle \left\langle B_{mnpq} \right\rangle^{-1} \left\langle \Phi_{pq} \right\rangle + \left\langle M_{ijkl}\,\Phi_{kl} + \dot{\varepsilon}_{ij}^{do} \right\rangle. \end{aligned} \tag{D12}$$

Hence,

$$\overline{M}_{ijpq} = \left\langle M_{ijkl}\, B_{klmn} \right\rangle \left\langle B_{mnpq} \right\rangle^{-1} , \tag{D13}$$

$$\dot{E}_{ij}^{do} = \left\langle M_{ijkl}\, \Phi_{kl} + \dot{\varepsilon}_{ij}^{do} \right\rangle - \left\langle M_{ijkl}\, B_{klmn} \right\rangle \left\langle B_{mnpq} \right\rangle^{-1} \left\langle \Phi_{pq} \right\rangle . \tag{D14}$$

The self-consistent equations (D13) and (D14) represent a generalization of Eq. (67). As for the spherical components, using (D6b), we obtain

$$\dot{\varepsilon}^{s} = \frac{\overline{K} + \tilde{K}}{K + \tilde{K}} \dot{E}^{s\bullet} , \tag{D15}$$

from where, averaging,

$$\dot{E}^{s} = \left\langle \frac{\overline{K} + \tilde{K}}{K + \tilde{K}} \right\rangle \dot{E}^{s\bullet} . \tag{D16}$$

If every grain has the same shape and every void has the same shape (but different from each other), only two different values of the Eshelby factor have to be considered: Ψ_g and Ψ_v respectively. The grain and void interaction tensors associated with the compressibility are given by Eq. (57c) as

$$\tilde{K}_v = \frac{1-\Psi_v}{\Psi_v} \overline{K} , \tag{D17a}$$

$$\tilde{K}_g = \frac{1-\Psi_g}{\Psi_g} \overline{K} , \tag{D17b}$$

while for incompressible grains and infinitely compressible voids we have

$$\frac{\overline{K} + \tilde{K}}{K + \tilde{K}} = \begin{cases} 0 & \text{for grains } (K \to \infty) , \\ \dfrac{\overline{K} + \tilde{K}_v}{\tilde{K}_v} & \text{for voids } (K = 0) . \end{cases} \tag{D18}$$

As a consequence,

$$\left\langle \frac{\overline{K} + \tilde{K}}{K + \tilde{K}} \right\rangle = \frac{\phi}{1-\Psi_v} , \tag{D19}$$

from where (D16) becomes

$$\dot{E}^{s\bullet} = \frac{1-\Psi_v}{\phi}\,\dot{E}^{s} \ . \tag{D20}$$

Replacing (D20) in (D15) to remove the auxiliary strain rate $\dot{E}^{s\bullet}$,

$$\dot{\varepsilon}^{s} = \frac{1-\Psi_v}{\phi}\,\frac{\overline{K}+\tilde{K}}{K+\tilde{K}}\,\dot{E}^{s} \ . \tag{D21}$$

Then,

$$\overline{K}\,\dot{E}^{s} = \Sigma^{s} = \left\langle \sigma^{s} \right\rangle = \left\langle K\dot{\varepsilon}^{s} \right\rangle = \frac{1-\Psi_v}{\phi}\left\langle \frac{K}{K+\tilde{K}}\left(\overline{K}+\tilde{K}\right)\right\rangle \dot{E}^{s} \ . \tag{D22}$$

Using Eq. (71) in (D22),

$$\overline{K} = \frac{1-\Psi_v}{\phi}\,(1-\phi)\left(\overline{K}+\tilde{K}_g\right) , \tag{D23}$$

which, combined with (D17b), leads to the following self-consistent equation for the determination of the viscoplastic bulk modulus $\overline{K}$:

$$\overline{K} = \frac{1-\phi}{\phi}\ \frac{1-\Psi_v}{\Psi g}\,\overline{K} \ . \tag{D24}$$

APPENDIX E. SCALING OF THE STRESS TO MATCH A REFERENCE DISSIPATION RATE IN VPSC

The dissipation rate is given by

$$\dot{W} = \Sigma_{ij}\,\dot{E}_{ij} \ . \tag{E1}$$

Decomposing the tensors in the deviatoric and spherical components

$$\dot{E}_{ij} = \dot{E}^{d}_{ij} + \dot{E}^{s}_{ij} = \dot{E}^{d}_{ij} + \frac{\dot{E}^{s}}{3}\delta_{ij} \ , \tag{E2}$$

$$\Sigma_{ij} = \Sigma^{d}_{ij} + \Sigma^{s}_{ij} = \Sigma^{d}_{ij} + \Sigma^{s}\delta_{ij} \ , \tag{E3}$$

allows us to rewrite (E1) as

$$\dot{W} = \Sigma^{d}_{ij}\,\dot{E}^{d}_{ij} + \Sigma^{s}\,\dot{E}^{s} \ . \tag{E4}$$

We want to show that given a reference state $\Sigma^{ref}_{ij}, \dot{E}^{ref}_{ij}$, then, if a stress state Σ^{0}_{ij} such that

$$\Sigma^{0}_{ij} = \lambda\Sigma^{ref}_{ij} \tag{E5}$$

is applied to the polycrystal, the resultant strain rate will be

$$\dot{E}^{0}_{ij} = \lambda^{n}\,\dot{E}^{ref}_{ij} \ . \tag{E6}$$

Equation (E5) can be written separately for the deviatoric and spherical stress tensors

$$\Sigma^{d,0}_{ij} = \lambda\,\Sigma^{d,ref}_{ij} \ , \tag{E7}$$

$$\Sigma^{s,0}_{ij} = \lambda\,\Sigma^{s,ref}_{ij} \ . \tag{E8}$$

It is easy to show that Eq. (E6) holds true for the deviatoric tensors. Using the connection between local and macroscopic strain rate and the homogeneity of order *n* of local deviatoric constitutive equation (53a), we have

$$\dot{E}^{d,0}_{ij} = \dot{E}^{d,0}_{ij}(\Sigma^{d,0}_{ij}) = \dot{E}^{d,0}_{ij}(\lambda\Sigma^{d,ref}_{ij}) = \left\langle \dot{\varepsilon}^{d,0}_{ij}(\lambda\sigma^{ref}) \right\rangle = \lambda^{n}\left\langle \dot{\varepsilon}^{d,ref}_{ij}(\sigma^{ref}) \right\rangle =$$
$$= \lambda^{n}\,\dot{E}^{d,ref}_{ij} \ . \tag{E9}$$

If the same relation holds for the spherical components

$$\dot{E}_{ij}^{s,0} = \lambda^n \Sigma_{ij}^{s,ref} \tag{E10}$$

or

$$\dot{E}^{s,0} = \lambda^n \Sigma^{s,ref} \ , \tag{E11}$$

then the dissipation rate of both the states is related by

$$\dot{W}^0 = \Sigma_{ij}^{d,0} \ \dot{E}_{ij}^{d,0} + \Sigma^{s,0} \ \dot{E}^{s,0} = \lambda^{n+1} \ \Sigma_{ij}^{d,ref} \ \dot{E}_{ij}^{d,ref} + \lambda^{n+1} \ \Sigma^{s,ref} \ \dot{E}^{s,ref} =$$
$$= \lambda^{n+1} \ \Sigma_{ij}^{\ ref} \ \dot{E}_{ij}^{\ ref} = \lambda^{n+1} \ \dot{W}^{ref} . \tag{E12}$$

Hence, given an arbitrary stress and associated strain rate, the correction to the stress that gives a state with the reference dissipation rate $\dot{W}^{ref}$ is

$$\Sigma_{ij}^{ref} = \left(\frac{\dot{W}^{ref}}{\dot{W}^o} \right)^{\frac{1}{n+1}} \Sigma_{ij}^o \ . \tag{E13}$$

For verification purposes, in Fig. E1 we present the results of running VPSC for the case of a random fcc polycrystal when varying the norm of the applied stress for two different cases of fixed porosity, triaxiality, and rate sensitivity. We plot there the quadratic norms of the deviatoric and spherical stress tensors versus the quadratic norms of the deviatoric and spherical strain-rate tensors respectively and the dissipation rate versus the quadratic norm of the Cauchy stress tensor. From the linearity and the slopes of the log-log plots, it can be seen that the curves corresponding to the deviatoric and spherical norms are consistent with Eqs. (E9) and (E10), respectively, and as a consequence, the dissipation rate fulfills the relation (E13). Although these results were derived for only two sets of parameters, we have verified that these results are independent of the choice of parameters.

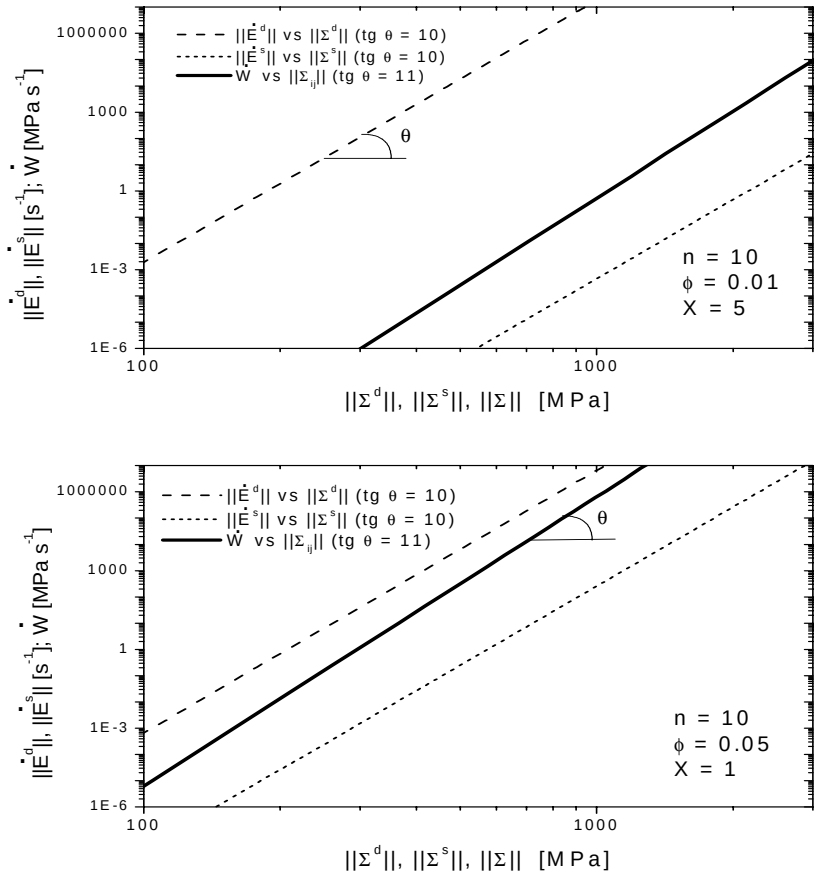

Figure E1. Plots of deviatoric and spherical stress tensor norms ($\left\|\Sigma_{ij}^{d}\right\|$ *and* $\left\|\Sigma_{ij}^{s}\right\|$*, respectively) versus deviatoric and spherical strain-rate tensor norms (* $\left\|\dot{E}_{ij}^{d}\right\|$ *and* $\left\|\dot{E}_{ij}^{s}\right\|$*, respectively) and dissipation rate* $\dot{W}$ *versus Cauchy stress norm* $\left\|\Sigma_{ij}\right\|$ *for the case of a random fcc polycrystal with a rate-sensitivity exponent n = 10,* τ^s *= 100 Mpa, and for two sets of porosity and triaxiality. The log-log plots have constant slopes equal to n for the deviatoric and spherical stress norms and (n + 1) for the dissipation rate, indicating dependences of the type (E9), (E10), and (E13), respectively. Same behavior is obtained for arbitrarily chosen porosities, triaxialities, rate sensitivities, and textures.*

Los Alamos NM 87545